https://doi.org/10.5194/egusphere-2025-5209
Preprint. Discussion started: 11 February 2026

Model Assessment of Winter Extratropical Cyclone Short-Term Impacts on the Antarctic Marginal Ice Zone

Noah S. Day[1], Siobhan P. O'Farrell[2], and Luke G. Bennetts[1]

[1]School of Mathematics and Statistics, The University of Melbourne, 3010, Melbourne, Victoria, Australia
[2]CSIRO Environment, Commonwealth Scientific and Industrial Research Organisation, 3195, Aspendale, Victoria, Australia

Correspondence: Noah S. Day (noah.day@unimelb.edu.au)

Abstract. The Antarctic marginal ice zone (MIZ) is the transitional region between the Antarctic sea ice edge and the consolidated ice cover, which is characterised by the presence of ocean surface waves and relatively small ice floes, and is a region where atmospheric and oceanic processes strongly influence sea ice dynamics. Extratropical polar cyclones intensify these processes by amplifying wave activity, transporting heat and moisture, and driving sea ice drift across the MIZ. Here, the CICE sea ice model with a wave propagation module is used at a 0.25° resolution to analyse statistically the impact of ∼400 cyclones on the location of the Antarctic ice edge and MIZ width. Cyclone-driven winds cause sudden shifts of ∼20 km in the ice edge location, through both compaction and expansion, with expansion events more effective in early winter and compaction later. MIZ widening is primarily driven by short-lived, major wave-induced breakup events, which increase the MIZ width by ∼30 km on average, with greater breakup associated with greater widening. Extreme ice edge changes result from the combined influence of sea ice drift and thermodynamics, whereas extreme MIZ width changes are primarily governed by the presence or absence of wave activity. These findings highlight the varied yet pronounced responses of the Antarctic MIZ to extratropical cyclones and underscore the critical role of waves in shaping the boundary between the MIZ and the consolidated ice pack, reinforcing the need to account for wave impacts in future studies.

1 Introduction

The Antarctic marginal ice zone (MIZ) is the outermost region of the Southern Ocean sea ice cover, situated between the sea ice edge and the consolidated inner ice pack, and where energetic long-period swell from the Southern Ocean regularly influence sea ice properties over tens to hundreds of kilometres (Kohout et al., 2014; Bennetts et al., 2024). The MIZ is also characterised by a unconsolidated, granular ice cover, containing relatively small, thin ice floes, which is largely due to wave-induced breakup of larger ice floes and wave action preventing newly formed floes from consolidating (Vichi et al., 2019; Alberello et al., 2020). In particular winter, when the Antarctic MIZ is at its widest (Brouwer et al., 2022; Fraser et al., 2025), the MIZ is dominated by pancake ice floes, separated by brash and frazil ice (Alberello et al., 2019). Owing to its distinctive ice cover, the MIZ modulates momentum and heat exchanges between the atmosphere and ocean (Vihma et al., 2014; Renfrew et al., 2021; Tersigni et al., 2023), shaping the seasonal evolution of the Antarctic sea ice system (Eayrs et al., 2019; Hobbs et al., 2024) and playing a key role in both the advance and retreat of the ice edge (Kimura et al., 2022; Himmich et al., 2023).

https://doi.org/10.5194/egusphere-2025-5209
Preprint. Discussion started: 11 February 2026

The location, width and ice properties of the Antarctic MIZ exhibit substantial variability (Bennetts et al., 2022a; Massom et al., 2025; Fraser et al., 2025), which is associated with its unique ice properties – thin, small, and unconsolidated floes – that enhance physical processes such as elevated melt rates (Horvat et al., 2016; Bennetts et al., 2017; Day et al., 2024) and rapid ice drift driven by winds (Alberello et al., 2020; Womack et al., 2022, 2024; Day et al., 2024). Extratropical cyclones, which are more frequent in winter than summer (Simmonds and Keay, 2000a), intensify these processes by transporting heat and moisture to high latitudes (Simmonds and Keay, 2000b), while generating powerful winds and large waves (Vichi et al., 2019; Alberello et al., 2022). Cyclones can induce intense rotational drift of sea ice across spatial scales of several hundred kilometres within only a few days (de Jager and Vichi, 2022), while simultaneously generating waves that fracture the consolidated inner ice pack (Doble and Bidlot, 2013; Kohout et al., 2016), thereby expanding the MIZ (Vichi et al., 2019). Nevertheless, the contributions of cyclone-enhanced processes in determining the width of the Antarctic MIZ remains poorly quantified. Advancing this understanding is critical, as climate projections indicate a stormier Southern Ocean and a greater occurrence of extreme wave events (Meucci et al., 2020; Young et al., 2020).

Most research concerning cyclone impacts on sea ice has examined major ice-loss events, with a strong focus on the Arctic (Kriegsmann and Brümmer, 2014; Wang et al., 2020; McGraw et al., 2022), motivated by observational case studies demonstrating their strong influence on sea ice concentration and their potential contributions to the rapid decline of Arctic sea ice (Brümmer et al., 2008; Holland et al., 2008; Asplin et al., 2014). Recent studies have increasingly highlighted the role of cyclones in driving key Arctic MIZ processes (Smith et al., 2018; Clancy et al., 2021; Blanchard-Wrigglesworth et al., 2022; Mundi and L'Ecuyer, 2024). In the Southern Ocean, cyclone activity has been linked to synoptic-scale variations in Antarctic sea ice extent near the ice edge (Matear et al., 2015; Schroeter et al., 2017; Hepworth et al., 2024). However, understanding of the role of waves in these processes remains limited, relying largely on isolated observations of large waves penetrating long distances into the Antarctic sea ice during cyclone events (Vichi et al., 2019; Alberello et al., 2022; Jena et al., 2022). The reliance on sparse measurements leaves a critical gap in quantifying the frequency, intensity, and impacts of MIZ-specific wave–ice interactions on Antarctic sea ice (Bennetts et al., 2022a).

Evidence from Arctic studies shows that cyclones can drive sea ice divergence near the ice edge, where the MIZ meets the open ocean. Depending on the season, this can either enhance melting (Zhang et al., 2013; Kriegsmann and Brümmer, 2014) or promote ice-edge advance (Smith et al., 2018). More subtle impacts have also been reported, including suppressed ice growth (Graham et al., 2019) and slowed ice loss (Finocchio et al., 2020), which complicate interpretations further. The magnitude of these impacts on sea ice concentrations (and consequently the ice edge location) are strong, yet they exhibit opposing effects on either side of the cyclone. It follows that averaging over large spatial domains may obscure the true magnitude of these contributions (Clancy et al., 2021).

The complexity of processes heightened by cyclone activity makes dynamic–thermodynamic numerical models, such as the Community Ice CodE (CICE; Hunke et al., 2021), powerful tools for quantifying impacts, as they resolve many relevant processes explicitly. Earlier versions of CICE have been used to simulate cyclone-driven rapid ice loss events in the Arctic (Clancy et al., 2021; Lukovich et al., 2021; McGraw et al., 2022), while the latest major release (version 6) incorporates key MIZ dynamics, including wave-induced breakup, pancake ice formation, and lateral melt (Roach et al., 2019). These processes govern

https://doi.org/10.5194/egusphere-2025-5209
Preprint. Discussion started: 11 February 2026

the evolution of a floe size distribution (FSD; Horvat and Tziperman, 2015; Roach et al., 2018a), which is a critical indicator of MIZ-like conditions, such as the presence of waves (Dumont, 2022; Day et al., 2024).

In this article, we use CICE6 with a waves-in-ice module to study the response of Antarctic sea ice to the extratropical cyclones that cross the MIZ. Building on previous studies, we analyse hourly outputs in track-localised domains to capture the contributions of the rapid processes that impact the Antarctic MIZ (Vichi et al., 2019; Clancy et al., 2021; Blanchard-Wrigglesworth et al., 2022; Mundi and L'Ecuyer, 2024). We use a dataset of cyclone tracks (Phillips, 2020) to identify areas of the MIZ impacted by cyclones. Our analysis focusses on the evolution of sea ice properties in the MIZ and the changes in the location of its boundaries, which determine its width, driven by three primary processes: thermodynamic processes (melting and freezing of sea ice), sea ice drift, and wave-induced ice breakup. The processed catalogue of 396 cyclone tracks enables a two-part study: (i) case studies on the roles of thermodynamics, ice drift, and waves (§3); and (ii) a statistical analysis of the expected and seasonal responses of the MIZ width, including the location of the ice edge (§4). The latter includes conditions that promote different responses in the MIZ and attribution of extreme MIZ changes to processes. Together, these findings provide novel insights into the roles of sea ice thermodynamics and dynamics (including waves) in shaping the outer margins of the Antarctic sea ice cover.

2 Methods

2.1 Numerical Sea Ice Model (CICE6-WIM)

This study uses the CICE6 numerical sea ice model with a waves-in-ice module (CICE6-WIM). CICE6 (version 6.2.0) evolves the thickness, h, and floe size (radius), r, as a joint distribution, $f(\mathbf{x}, t; r, h)$, through space, $\mathbf{x}$, and time, t. Given a floe size and thickness, the areal sea ice concentration is given by $f(r,h)\mathrm{d}r\mathrm{d}h$ (Roach et al., 2018a), where $\mathrm{d}r$ and $\mathrm{d}h$ correspond with the width of the respective floe size and thickness categories.

Sea ice area in CICE6 is evolved through the governing equation (Horvat and Tziperman, 2015)

$$\frac{\partial f(r,h)}{\partial t} = -\nabla \cdot (f(r,h)\mathbf{u}) + \mathcal{L}_T + \mathcal{L}_M + \mathcal{L}_W$$

where the terms on the right-hand side correspond with advection, thermodynamics, mechanical deformation, and wave-induced processes, respectively. The horizontal velocity of sea ice, $\mathbf{u}$, is solved by a 2D momentum equation (Hibler III, 1979) with an elastic-viscous-plate rheology (Hunke and Dukowicz, 1997).

Sea ice loss through thermodynamic processes occurs via three modes: basal, surface (top), and lateral melt. In contrast, thermodynamic ice growth is classified as either frazil or congelation, which contribute to increases in sea ice area (through lateral growth and new floe formation) or thickness, respectively. Waves impact the floe size distribution by breaking existing floes into smaller fragments and by limiting the size of newly formed floes (Roach et al., 2019; Shen et al., 2001; Horvat and Tziperman, 2015). Mechanical processes, however, do not directly affect the floe size distribution.

The WIM propagates waves southward along meridional lines into the Antarctic ice cover on an hourly timescale. Significant wave height, H_s, and peak period, T_p, are taken from a WAVEWATCH III hindcast (Smith et al., 2021) and the spectral density

https://doi.org/10.5194/egusphere-2025-5209
Preprint. Discussion started: 11 February 2026

function, $S(\omega)$, is initialised according to a Bretschneider spectrum (Bretschneider, 1959)

$$S_{\text{in}}(\omega) = \frac{5}{32\pi} H_s^2 \frac{T^5}{T_p^4} e^{-\frac{5}{4}\left(\frac{T}{T_p}\right)^4},$$

where $\omega = 2\pi/T$ is the angular wave frequency. The propagated wave spectrum at cell i, denoted $S_i(\omega)$, is exponentially attenuated through the ice cover (Golden et al., 2020; Bennetts, 2025), so that

$$S_i(\omega) = S_{\text{in}}(\omega) e^{-a_{\text{ice}}\alpha(\omega)\Delta x},$$

the attenuation coefficient $\alpha(\omega) = c_1\omega^2 + c_2\omega^4$ is derived from the empirical model of Meylan et al. (2014) and scaled by the areal ice concentration, a_{ice}. The distance from the ice edge to cell i is given by Δx. The WIM neglects both directional wave propagation as well as wave generation within the sea ice.

2.2 Model Configuration

The simulation is conducted on a tripolar medium resolution grid for 2005–2018, where the first five years (2005–2009) is discarded to allow the model to spin-up. The resolution of 0.25° (latitude–longitude) is chosen to capture the mesoscale to synoptic scale response of the MIZ to the most intense cyclones (e.g., Vichi et al., 2019), which typically range from 3–6° in latitude (Uotila et al., 2011). Atmospheric forcing is provided by JRA55-do 1.4.0 (Tsujino et al., 2018), oceanic forcing by ACCESS-OM2 (Kiss et al., 2020), and wave forcing by the CAWCR Wave Hindcast reanalysis (Smith et al., 2021). Atmospheric and oceanic data are interpolated onto the model timestep (one hour) from their native 3-hourly and monthly frequencies, respectively. The wave forcing is available at an hourly resolution, and, hence, is used without need for further temporal interpolation. Horizontally, atmospheric and wave datasets are interpolated from resolutions of 0.5° and 0.4°, respectively, to match the model grid of 0.25°. The CAWCR Wave Hindcast is forced with surface winds and sea ice fields from the Climate Forecast System (version 2; Saha et al., 2014). Hourly model outputs from July to November of 2015–2018 are analysed, generating 4.5 TB of data. The analysis of hourly outputs at synoptic scales is chosen to capture the sensitivity of cyclone-driven sea ice processes near the cyclone centre (Clancy et al., 2021), during months when intense cyclones have been observed to impact the MIZ (Vichi et al., 2019).

2.3 Cyclone Identification

The cyclone track dataset from Phillips (2020) is used to identify the times and locations where cyclones pass over the Antarctic MIZ. The dataset was generated using the University of Melbourne cyclone tracking algorithm (Keay et al., 2020) applied to 6-hourly ERA-Interim reanalyses (Dee et al., 2011) from 1979 to 2018, and has been widely used in previous studies of similar scope (Sprenger et al., 2017; Clancy et al., 2021; Blanchard-Wrigglesworth et al., 2021). Here, extratropical cyclones are identified based on selection criteria requiring genesis north of 60° S, and classification as "strong closed" by the tracking algorithm, which means each cyclone exhibits a well-defined closed sea level pressure depression with strong vorticity (see Keay et al., 2020). Since stronger cyclones are more consistently identified across reanalyses (Grieger et al., 2018), this restriction enhances the robustness of the selection. To exclude larger systems, which are generally less intense (Uotila et al., 2011), only

https://doi.org/10.5194/egusphere-2025-5209
Preprint. Discussion started: 11 February 2026

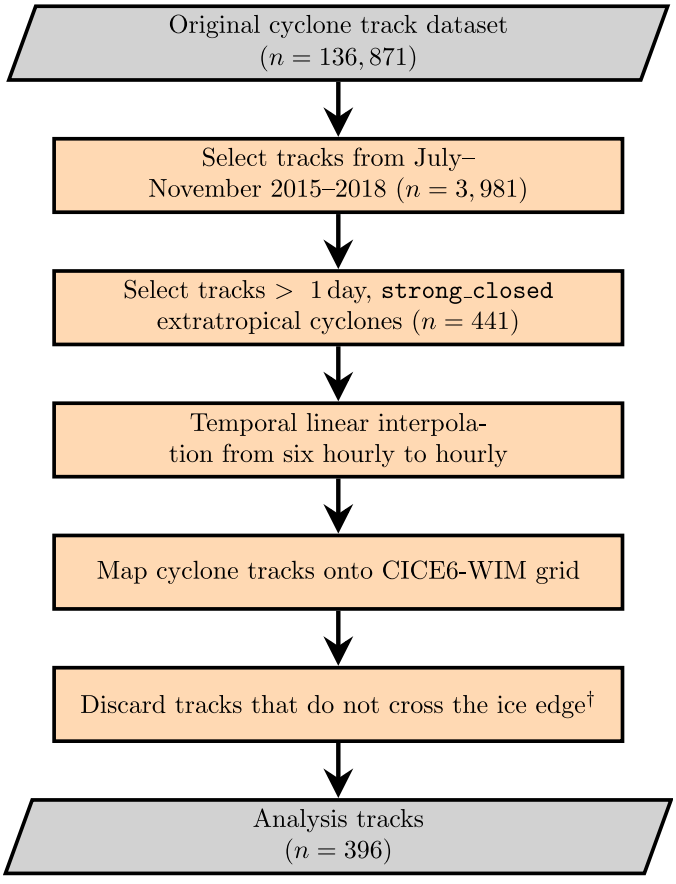

Figure 1. Process of selecting cyclone tracks from the cyclone track dataset (Phillips, 2020). The number of cyclone tracks is selected to ensure that only well-defined storms interacting with the Antarctic sea ice edge are considered. †Tracks with mean sea level pressures which disagree with JRA55-do by more than 10 hPa are also discarded.

cyclone tracks that at any time come within 600 km of the CICE6-WIM modelled ice edge are considered. This threshold has previously been shown to be effective for identifying relationships between cyclones and atmospheric anomalies (Hepworth et al., 2022) and sea ice variability (Hepworth et al., 2024). To define a trajectory, each cyclone track is required to persist for at least 24 hours (four track points), which identifies more intense cyclones, characterised by lower central pressure minima and a greater Laplacian of central pressure (i.e., factors used in the strength criteria of Keay et al., 2020). The cyclone track selection technique was evaluated against cyclone statistics to ensure that it did not introduce biases in spatial distribution, central pressure, or cyclone radius (not shown).

https://doi.org/10.5194/egusphere-2025-5209
Preprint. Discussion started: 11 February 2026

2.4 Forcing Data Preparation and Consistency Analysis

CICE6-WIM outputs are used to investigate the evolution of the Antarctic ice edge and MIZ width in response to the crossing of cyclones. For each cyclone, sectors with arc lengths of approximately 580 km (or 21 grid cells wide) are selected around the location where the cyclone intersects the modelled ice edge (referred to as the “cyclone crossing location"), meaning that these sectors are fixed in space. Each subdomain is analysed over the duration of the corresponding cyclone.

To align with the CICE6-WIM timestep, JRA55-do is linearly interpolated to an hourly frequency. Consequently, cyclone tracks are also interpolated to map the 6-hourly cyclone positions onto the model outputs. For each track, a sector of the sea ice is targetted that will be exposed to a polar cyclone at a given time. The minimum sea level pressure from JRA55-do determines when the cyclone crosses the ice edge. In other words, the track informs our method of the cyclone location, but the atmospheric forcing is used to derive the time the cyclone crosses the ice edge. Following this identification, the cyclone track dataset becomes redundant, as it only serves to inform the sectors and times where a cyclone crossing is likely. Therefore, all atmospheric fields presented are from JRA55-do.

As mentioned earlier, JRA55-do is used to force the atmospheric conditions in CICE6-WIM, while the wave hindcast produced by CAWCR is based on the Climate Forecast System version 2 (CFSv2) reanalysis (Saha et al., 2014). Thus, a comparison is conducted between JRA55-do and CFSv2 to assess the consistency between the two sources of atmospheric forcing. Figures A1–A3 in Appendix A show strong agreement in sea level pressure and moderate consistency in the wind components. The results in Sections 3–4 are intended to be considered in the context of wave-induced breakup coinciding with cyclones crossing the MIZ, rather than the contribution of the cyclone-generated waves on the breakup of sea ice.

2.5 Quantifying the Antarctic Marginal Ice Zone Extent

The outer MIZ boundary (ice edge) is identified using the standard 15% sea ice concentration threshold, such that $a_i \geq 0.15$, where a_i denotes the areal sea ice concentration obtained by integrating $f(r,h)$ over all considered radii, $\mathcal{R}$, and thicknesses, $\mathcal{H}$. The inner MIZ boundary (transition to consolidated ice pack) is identified using a representative floe size threshold, $r_a < 100$ m, where (Roach et al., 2018a)

$$r_a = \frac{1}{a_i} \int_{\mathcal{R}} \int_{\mathcal{H}} r\, f(r,h)\, \mathrm{d}h\, \mathrm{d}r. \tag{1}$$

For each longitude and time, the width of the Antarctic MIZ, d_{100}, is calculated along the meridional transect (indexed by j) from the grid cell corresponding to the outer boundary, c_{15}, to the cell correspondiung to the inner boundary, c_{100}. Thus,

$$d_{100} = \sum_{j=c_{15}}^{c_{100}} \Delta x_j,$$

where Δx_j denotes the meridional length of a grid cell at location j. The MIZ widths produced from this definition are reasonably consistent with more sophisticated definitions over winter–spring (e.g., Day et al., 2024, see comparison in Appendix B Fig. B1). Differences appear at the end of November, indicating the limited use of such a simple method.

https://doi.org/10.5194/egusphere-2025-5209
Preprint. Discussion started: 11 February 2026

3 Case Studies

3.1 Cyclone-Induced Heat Advection and Resulting Sea Ice Thermodynamics

A cyclone crossing the sea ice in the Bellingshausen Sea between 2 and 8 August 2015 is illustrated in Figure 2. The cyclone intensifies as it approaches the ice-covered region, with central pressure dropping from 960 to 930 hPa over 24 hours. The cyclone reaches its minimum pressure at the time of the crossing, which is accompanied by a steepening pressure gradient, as indicated by the compacted isobars. Sea ice in the MIZ is thin (∼0.15 m), with concentrations around 80% at the time of the cyclone crossing (see Appendix C, Fig. C1). Warm surface air advects over the sea ice (Fig. 2a–c), raising the surface temperature above the melting point (Fig. 2d–f) and heating the ocean surface. At this time, ice concentrations near the ice edge are low (∼40%), allowing enhanced ocean heat uptake and driving melt from both above and below the ice. The warming contributes to the retreat of recently formed ice (less than three weeks old), evidenced by an increase in average ice age of about one week over a two-day period. Following the cyclone crossing, surface temperatures cool, leading to substantial new ice formation and an increase in ice concentration near the ice edge from 40% to 70%.

In the MIZ near the cyclone, basal melt is the primary mode of ice loss, occurring when sea ice surface temperatures exceed the melting point prior to the cyclone's arrival at the ice edge (red shading in panel g). Basal melt exhibits periodic peaks that coincide with solar insolation, highlighting a diurnal signal in the MIZ's thermodynamic response. After the cyclone crosses the ice edge, surface temperatures decline, promoting new ice formation through both frazil and congelation processes at comparable rates. During the cyclone passage, the ice edge from 60.4° S to 61.1° S, while the inner MIZ boundary moves southward by only 0.4° (panel h). The retreat and subsequent rebound of the ice edge closely track periods of net ice melt and growth, respectively (red and blue shading in panel g), underscoring the role of thermodynamics in controlling ice edge location.

3.2 Rapid Expansion of the Ice Edge from Sea Ice Drift

From 2 to 9 August 2016, a cyclone travels across the Amundsen and Bellingshausen Seas, intersecting the ice edge near 86° W (Fig. 3a–c). Sea ice in this region is relatively thick (∼0.8 m) and at high concentrations (∼95%), effectively insulating the ocean from elevated air temperatures (see Appendix C, Fig. C2). As in the previous case, the cyclone intensifies while approaching the ice edge, reaching a minimum central pressure of 950 hPa. The cyclone, along with a secondary storm near ∼140° W, generates strong negative vorticity, which drives sea ice motion (Fig. 3d–f).

Unlike the previous case study, the cyclone follows a steady southward trajectory, approaching the Antarctic coastline. Its relatively linear path produces a clear division in sea ice drift within the MIZ, with southward drift on the eastern side and northward drift on the western side (Fig. 3g). The direction and magnitude of the meridional drift are closely aligned with the wind field (Fig. 3h). Wind-driven drift patterns persist both before and after the cyclone crossing, with southward drift preceding the event and northward drift following it. Shaded regions denote periods of consistent wind direction lasting at least six hours (within two days of the crossing) and capture the transition from on-ice to off-ice winds.

https://doi.org/10.5194/egusphere-2025-5209
Preprint. Discussion started: 11 February 2026

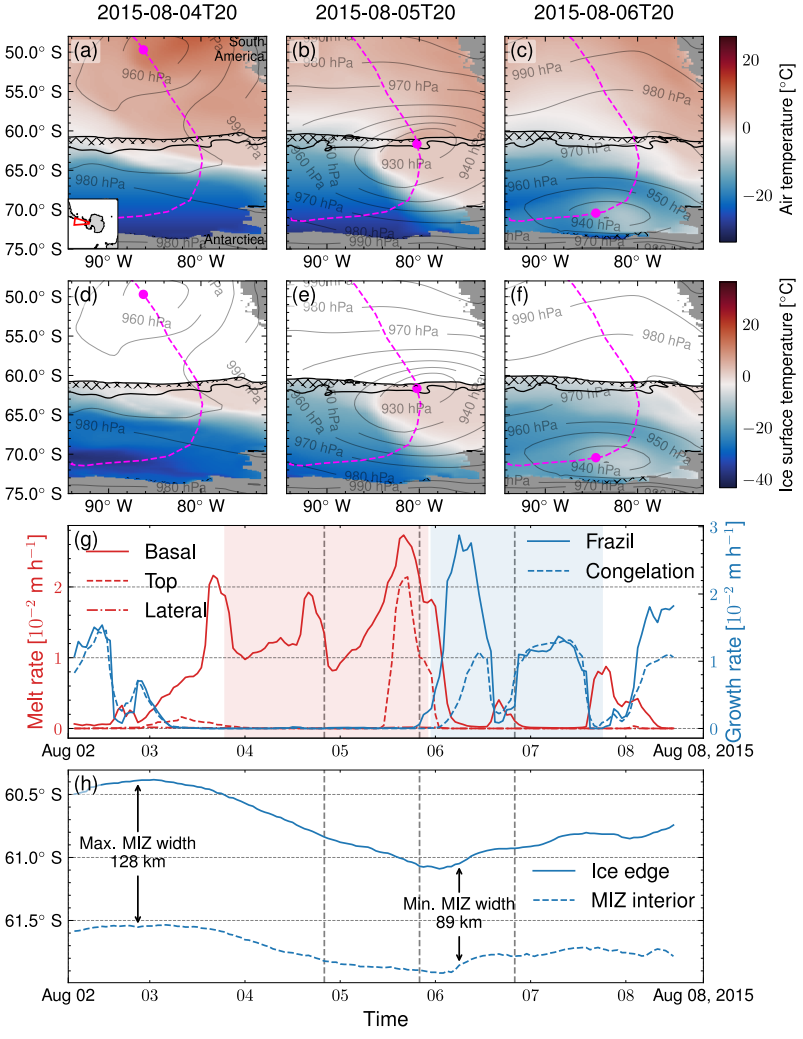

Figure 2. CICE6-WIM results for the impact of an extratropical polar cyclone on Antarctic sea ice melt and formation at ∼280° E from 2 to 9 August, 2015. (a–c) Forcing air temperature maps at 2 m for: (a) 24 hours before the cyclone's crossing, (b) at the time of crossing, and (c) 24 hours after, with colour bars centred around the freezing temperature of sea ice. Overlaid are isobars in 10 hPa intervals, plus the cyclone's location (magenta dot), and its track (dashed magenta line). Black contours indicate the boundaries of the MIZ and hatching marks the areas where the ice is less than three weeks old. Panels (d–f) correspond to (a–c) but show modelled ice surface temperature. (g) Time series of the modelled sea ice melt and growth rates, divided into basal, top, and lateral melt, and frazil and congelation growth, are presented. The data is averaged over the MIZ centred around the cyclone crossing location with melting and freezing events indicated in red and blue shading, respectively. (h) Time series of the ice edge location and inner MIZ locations.

Similar to the previous case study, the ice edge responds more strongly than the inner MIZ boundary (Fig. 3i). Here, the ice edge initially retreats by 0.5° as the cyclone approaches, followed by a rapid advance from 65.5° S to 63.9° S over two

https://doi.org/10.5194/egusphere-2025-5209
Preprint. Discussion started: 11 February 2026

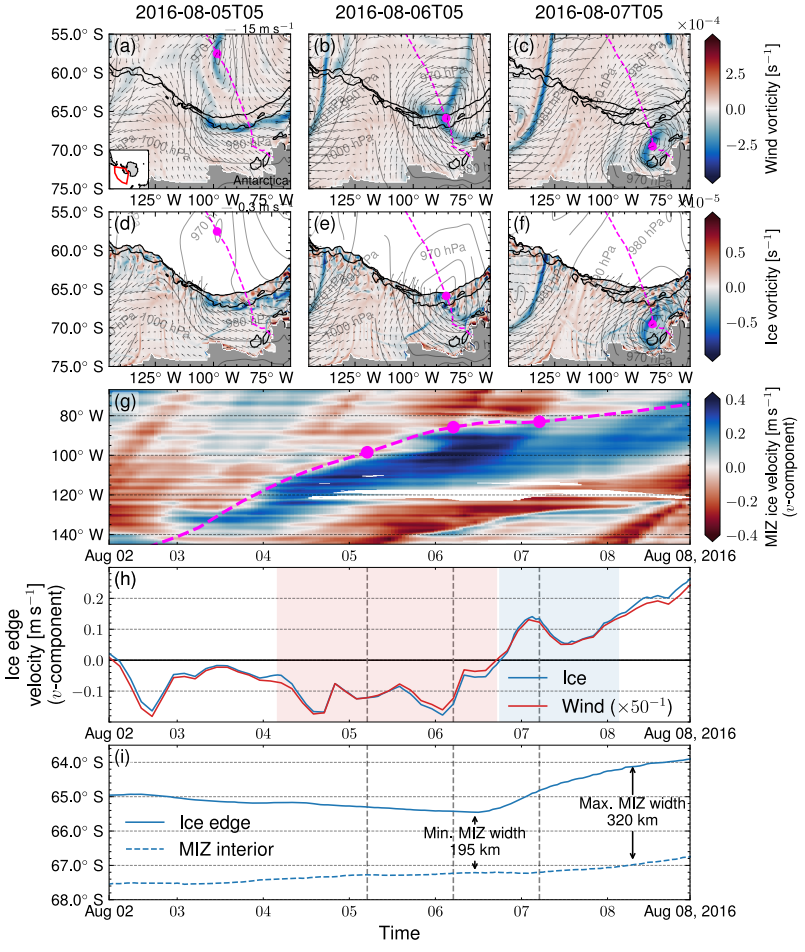

Figure 3. Similar to Figure 2 but for impacts of sea ice drift and ice edge location at ∼ 270° E from 2 to 9 August 2016. (a–c) Wind vorticity maps with wind velocity quivers over the crossing (similar to Fig. 2). Overlaid are isobars in 10 hPa intervals, plus the cyclone's location (magenta dot) and its track (dashed magenta line). Black contours indicate the boundaries of the MIZ. Panels (d–f) correspond to (a–c) but show ice vorticity with quivers representing ice drift. (g) Hovmöller diagram of the north–south sea ice velocity component averaged across the MIZ, along with the cyclone track and position at the snapshot times. (h) Time series of the east–west (red) and north–south (blue) ice and wind velocity components (solid and dashed lines, respectively), averaged over the MIZ centred around the cyclone crossing location. (i) Latitude of the ice edge and inner MIZ boundary over the same sector as in (h).

and a half days. These changes coincide with periods of consistent wind direction, suggesting that winds drive the ice edge
195 variability through sea ice drift.

https://doi.org/10.5194/egusphere-2025-5209
Preprint. Discussion started: 11 February 2026

3.3 Widening of the Antarctic MIZ from Wave-Induced Breakup of Sea Ice

A cyclone located in Eastern Antarctica (∼40° E) crossing the MIZ over 6 to 10 October 2016 (Fig. 4). Unlike the more explosive cyclones shown in the previous case studies, this cyclone's central pressure decreases gradually, maintaining a low of 940 hPa for over 24 hours as it crosses the MIZ. This sustained intensity is associated with a larger storm radius, spanning more than 9° in latitude, compared to 6–7° for the earlier cyclones. Sea ice within the MIZ is moderately thick (∼0.35 m), with concentrations between 80–90% during the cyclone crossing (see Appendix C, Fig. C3)). In contrast to the previous two case studies, sea surface temperatures cool during the cyclone passage and warm afterwards. Zonal winds dominate the forcing, resulting in relatively weak meridional drift and indicating that different mechanisms govern the sea ice response during the event.

The distribution of floe sizes across the ice pack defines the MIZ in Figure 4, with a clear transition from the MIZ (yellow region) to the inner ice pack (green–blue region). Significant wave heights increase along the cyclone's path while it travels over the open ocean, then decrease as the system moves into the ice-covered region (Fig. 4a–b). Waves reach a peak height of 8.5 m at the ice edge (Fig. 4e), initiating sea ice fracture on the eastern side of the cyclone, where persistent northerly winds occur, as indicated by dotted hatching in panel (d). This wave-induced fracturing breaks up consolidated ice, causing the floe sizes of such ice to decrease and the ice to transition to MIZ. This wave-induced fracturing breaks up consolidated ice into smaller floes, transforming the area into MIZ (Fig.4a–c). As a result, the MIZ width increases from 90 km to 180 km (Fig. 4e). The rate of wave-induced breakup is quantified as the change in representative floe radius per hour (see Eq. 1). A threshold applied to this rate captures the widening of the MIZ (shaded region in panel e), with the classification criteria for this event discussed in §4.2.

After the cyclone exits the MIZ, the wave heights decrease, allowing the ice cover to reconsolidate and the MIZ width to narrow to approximately 130 km. The strongest example of consolidation occurs near ∼40° E, where large floes form rapidly in response to the absence of wave energy (cross-hatching in Fig. 4d). Floe welding also contributes to reconsolidation; however, unlike new floe formation, this process is parameterised independently of wave activity in the FSTD (Roach et al., 2018a). Notably, the default welding rate in CICE6 (and in CICE6-WIM) is several orders of magnitude lower than the rate estimated by Roach et al. (2018b), which could introduce uncertainty in the timescales associated with MIZ narrowing through re-consolidation.

4 Statistical Results

4.1 Sea Ice Response to Cyclones Crossing the Marginal Ice Zone

Figure 5 depicts how atmospheric and sea ice conditions at the ice edge evolve over time across 396 cyclone tracks. The sea level pressure minima correspond to the cyclone centre (panel a) being at the ice edge. Additional local minima, which typically occur more than 24 hours before or after the crossing, are likely caused by irregular cyclone paths, such as multiple ice-edge crossings or interactions with other low-pressure systems.

https://doi.org/10.5194/egusphere-2025-5209
Preprint. Discussion started: 11 February 2026

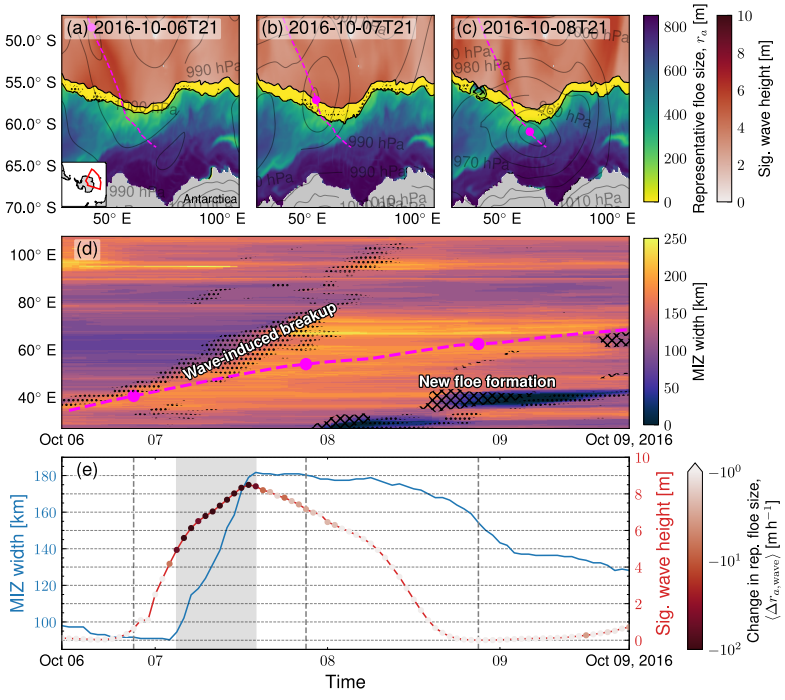

Figure 4. Similar to Figure 2 but for the impact of wave-induced sea ice breakup on the MIZ width at $\sim 50^\circ$ E from 6 to 10 October, 2016. (a–c) Representative floe size and significant wave height maps during the cyclone crossing (similar to Fig. 2) Overlaid are isobars in 10 hPa intervals, the cyclone's location (magenta dot), and its track (dashed magenta line). Black contours indicate the boundaries of the MIZ. Dotted- or cross-hatching indicates areas with a significant change in the representative floe size via wave-induced breakup or new floe formation, respectively. (d) Hovmöller diagram of the MIZ width, along with the cyclone track and position at the snapshot times. (e) Time series of the MIZ width (blue line) alongside the significant wave height at the ice edge (red line) with coloured dots indicating the amount of wave-induced breakup (from the edge to the coast). Vertical grey lines correspond with the snapshot times and shaded region denotes a major breakup event.

In mean (thick lines), there is a distinct shift in the north–south component of both wind and ice velocities near the cyclone centre, confirming the transition from the eastern to the western side of the system or from "on-ice" (northerly) to "off-ice" (southerly) winds (Fig. 5b–c). Before reaching the ice edge, cyclones typically advect warmer air over the sea ice ((Fig. 5d), which is then followed by sharp cooling after the cyclone centre passes (Fig. 5e).

Figure 6(a–b) shows the impacts of the cyclone crossings on the relative location of the ice edge and the width of the MIZ. The mean ice edge retreats by ∼30 km as the cyclone approaches and advances by ∼20 km afterwards, yielding a net retreat of ∼10 km. Ice edge retreat coincides with northerly winds and rising surface temperatures, which typically peak during the crossing, while the subsequent advance aligns with southerly winds and rapid cooling of both air and ice (Fig. 5b–e). Peaks in ice temperature correspond to suppressed new ice formation during the crossing, followed by enhanced formation afterward, consistent with surface temperature variations and patterns observed in the first case study (Fig. 6d).

https://doi.org/10.5194/egusphere-2025-5209
Preprint. Discussion started: 11 February 2026

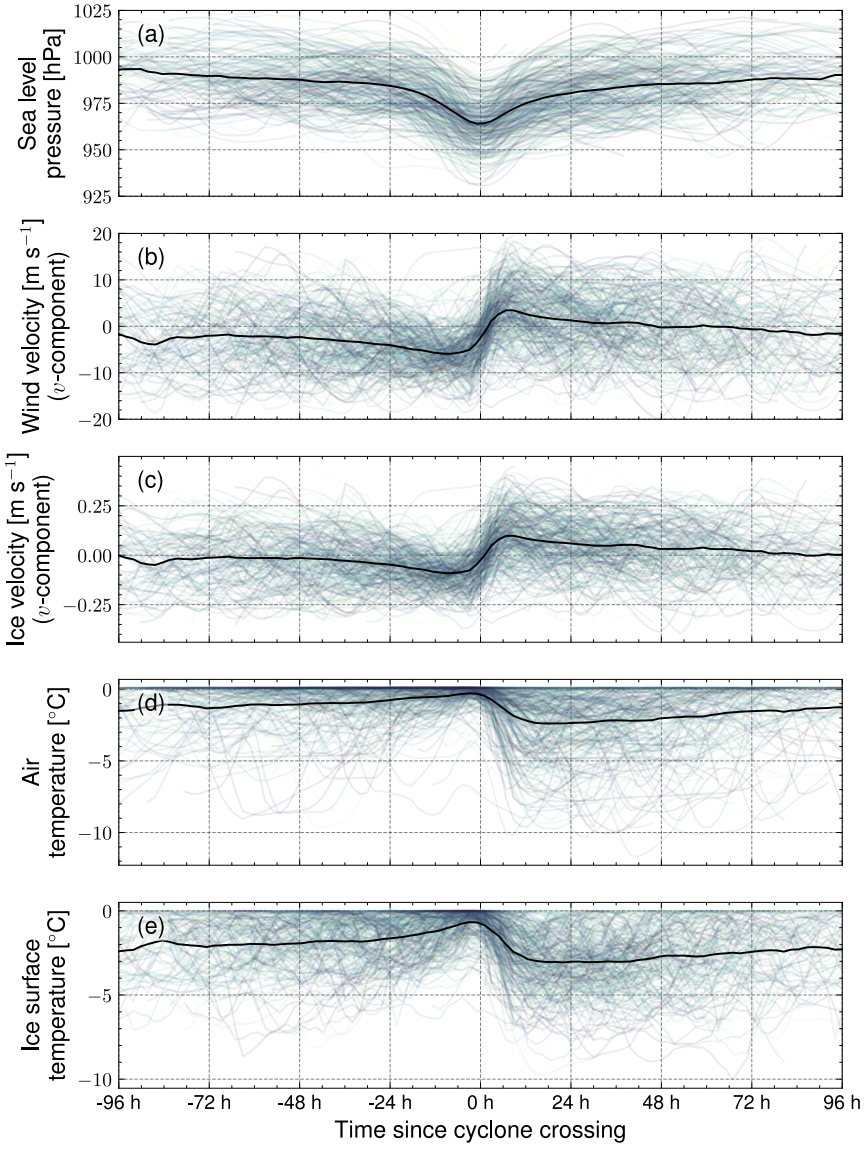

Figure 5. Time series of changes in atmospheric and sea ice conditions as extratropical cyclones cross the Antarctic sea ice edge: (a) sea level pressure; (b) north–south wind velocity; (c) north–south ice velocity; (d) air temperature; and (e) ice surface temperature, at the location where the cyclone crosses the ice edge. The thin grey lines represent 396 individual cyclones, with mean response shown in the thick black line.

The mean MIZ width narrows slightly during cyclone crossings. Unlike the ice edge, the MIZ exhibits greater variability, with rapid compactions and expansions throughout each cyclone's lifespan. Mean significant wave heights show no clear

https://doi.org/10.5194/egusphere-2025-5209
Preprint. Discussion started: 11 February 2026

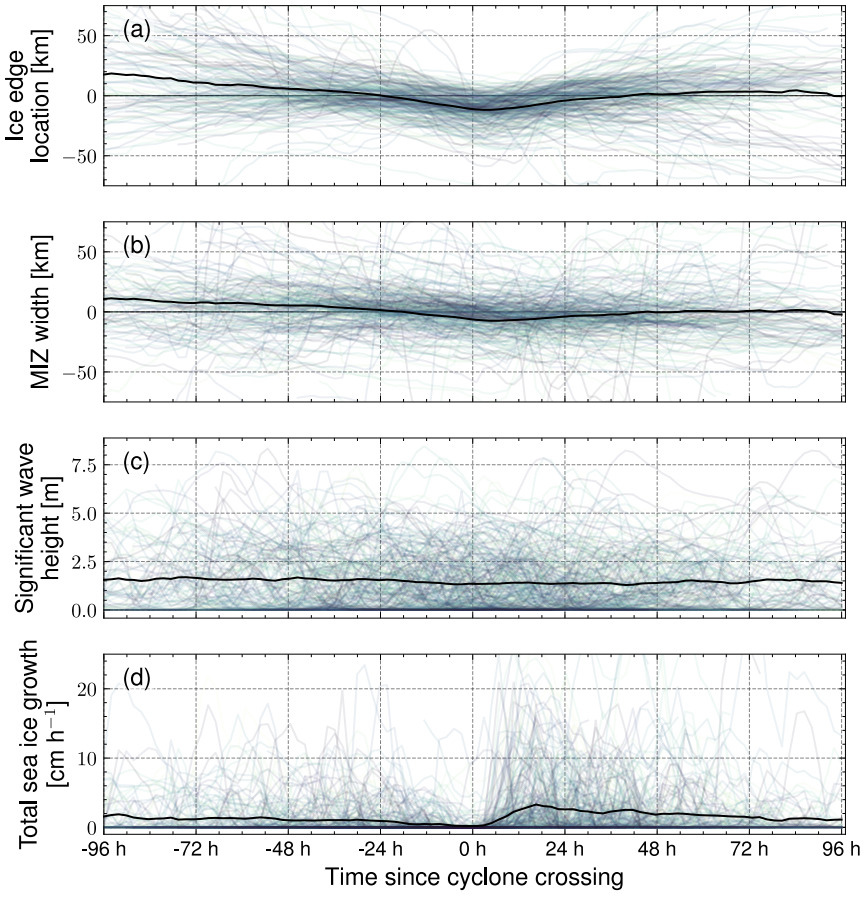

Figure 6. Time series depicting the effects of extratropical cyclones on the (a) relative north–south change in ice edge location and (b) the relative change in MIZ width, as well as (c) significant wave heights and (d) new sea ice formation. Times are centred on the cyclones' arrival at the ice edge. Relative changes are centred on the y-axis around their respective means. Sea ice growth is defined as the sum of congelation and frazil production.

relationship with cyclone proximity (Fig. 6c). Rather than responding predictably to the cyclone centre, wave heights and MIZ widths can shift abruptly, as illustrated by the third case study.

4.2 Categorisation of Cyclone-Induced Sea Ice Events

Due to the Coriolis effect, cyclonic winds in the Southern Hemisphere circulate clockwise (Lim and Simmonds, 2007). As a result, northerly winds on the eastern side of the cyclone transport heat southward. Similarly, after crossing the ice edge, southerly winds carry cold air from the ice-covered region northward, cooling the ice edge. This behaviour provides a consistent framework for tracking sea ice evolution within the MIZ. To identify wind-driven conditions, we define *on-ice wind events* as

https://doi.org/10.5194/egusphere-2025-5209
Preprint. Discussion started: 11 February 2026

periods when $v_{\text{wind}} < 0$ for at least six consecutive hours and *off-ice wind events* as periods when $v_{\text{wind}} > 0$ for the same duration. The net impact of these wind events is assessed by comparing conditions 24 hours before and after cyclone crossings.

We categorise thermodynamic events based on the ice surface temperature to isolate the effects of temperature changes on sea ice evolution. *Melting events* occurs when ice surface temperature (T_{ice}) exceeds $-1.8°\text{C}$ for at least six consecutive hours, while *freezing events* occur when T_{ice} falls below this threshold for a similar duration. This classification is used to highlight the role of cyclone-driven atmospheric forcing in modulating ice melting and formation.

Unlike wind and temperature, wave activity is less predictable relative to the cyclone's proximity to the ice edge (Fig. 6c). We do not assess the portion of wave energy attributable to cyclonic winds; instead, we examine waves coinciding with cyclone crossings of the ice edge. Given a latitude, longitude, and time, the contribution of wave-induced breakup to changes in the representative floe size is denoted as $\mathrm{d}r_{a,\text{wave}}/\mathrm{d}t$ (units of $\mathrm{m\,h^{-1}}$). The mean wave-induced breakup contribution per longitudinal transect over the sector of sea ice in the cyclone's proximity is then calculated as

$$\langle \Delta r_{a,\text{wave}} \rangle = \frac{1}{N_i} \sum_i \sum_j \frac{\mathrm{d}}{\mathrm{d}t} r_{a,\text{wave}}(i,j,t),$$

where the summation is performed over latitudes (j) and averaged over longitudes (i) across N_i grid cells within the analysis sub-domain. This formulation accounts for wave-induced breakup in the MIZ and the consolidated inner ice, which transitions to MIZ when sufficient breakup occurs (i.e., reducing to be $r_a < 100\,\text{m}$). *Major breakup events* are defined as periods when $\langle \Delta r_{a,\text{wave}} \rangle < -10\,\mathrm{m\,h^{-1}}$ for at least six consecutive hours, while *minor breakup events* refer to responses where $\langle \Delta r_{a,\text{wave}} \rangle > -10\,\mathrm{m\,h^{-1}}$. During minor breakup events, factors such as wind direction and air temperature are expected to play a more significant role in changes to MIZ width, as wave impacts are negligible.

Figure 7 shows the temporal distribution of the wind, thermodynamic, and wave events relative to cyclone crossings of the ice edge. On-ice winds generally precede cyclone crossings and coincide with melting events, while post-crossing off-ice winds are associated with freezing events. Minor breakup events occur more frequently than major ones, regardless of cyclone proximity. As expected from the sporadic nature of wave heights in Figure 6, no clear relationship emerges between the occurrence of breakup events and cyclone proximity to the ice edge.

4.3 Contribution of Wind and Thermodynamic Events on the MIZ and Ice Edge Location

The change in ice edge location and MIZ width per storm for on-ice winds, off-ice winds, and the net impact are shown in Figure 8(a–b). The median changes in the ice edge location are approximately $-10\,\text{km}$ and $10\,\text{km}$ for on- and off-ice wind events, respectively. Changes in MIZ width differ less between wind types: on-ice winds and the net impact typically cause a slight narrowing of about 5 km, whereas off-ice winds produce little change. These results indicate that ice edge retreat from on-ice winds can narrow the MIZ, but expansion from off-ice winds does not necessarily widen it.

Seasonality strongly influences the magnitude of the change in ice edge location (Fig. 8c). Melting and freezing events produce changes similar to on- and off-ice winds, consistent with the alignment between wind direction and thermodynamic forcing (Fig. 7). Although on- and off-ice wind events show considerable overlap in their impact on ice edge location (Fig. 8a), seasonal analysis reveals a growing prevalence of ice edge retreat as months progress, while a separation in the effect of the two

https://doi.org/10.5194/egusphere-2025-5209
Preprint. Discussion started: 11 February 2026

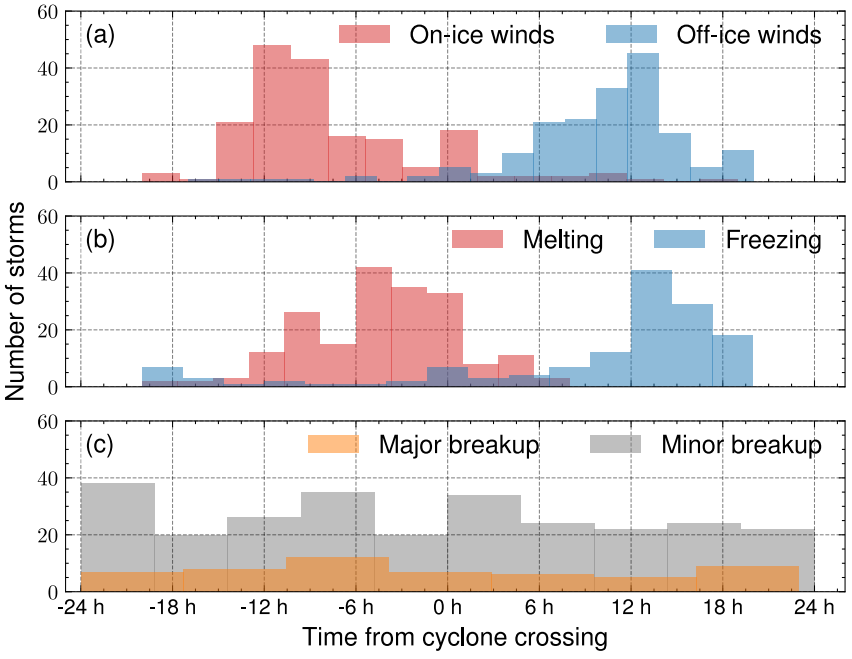

Figure 7. Temporal histograms showing the timing of (a) on- and off-ice wind events, (b) melting and freezing events, and (c) major and minor breakup events. Each event is aligned to the time at which the respective cyclone crossed the ice edge, with the plotted value representing its mid-time. Negative times indicate events occurring before the crossing, and positive times indicate events occurring after it.

event types persists. The sign of the net impact also exhibits seasonal dependence, with cyclones in July and August generally expanding the ice edge, whereas from September onwards, this reverses to compaction. The interquartile range includes zero for all months, indicating a wide spread in responses.

Figure 9 shows air and ice surface temperatures and total melt and growth rates for wind and thermodynamic events over winter. Off-ice winds are associated with cooler conditions, and on-ice winds with warmer conditions (panels a and b). It is evident that wind direction cannot account for these temperature changes entirely, likely due to the reduced wind intensity near the cyclone centre when temperatures generally peak (Fig. 7). Melt rates rise as winter progresses toward summer (panel c), driven primarily by basal melt, with lateral and surface melt one and two orders of magnitude smaller. This increase coincides with an increase in the melting potential (see Appendix D, Fig. D1), with basal melt dominating, while the lateral and surface melt rates are one and two orders of magnitude smaller, respectively. By November, melt during freezing events exceeds July–August melt during melting events, indicating heightened ice vulnerability. Growth rates (panel d) decline from September to November, enhanced by off-ice winds and freezing conditions but suppressed under melting conditions. The spread in growth rates is substantially greater than that observed for melting (Fig. 9c), suggesting a higher sensitivity to wind forcing and sea ice temperature during cyclones. Although growth and melt rates are comparable in July and August, melting dominates from September onwards, producing a net seasonal ice loss during cyclones.

https://doi.org/10.5194/egusphere-2025-5209
Preprint. Discussion started: 11 February 2026

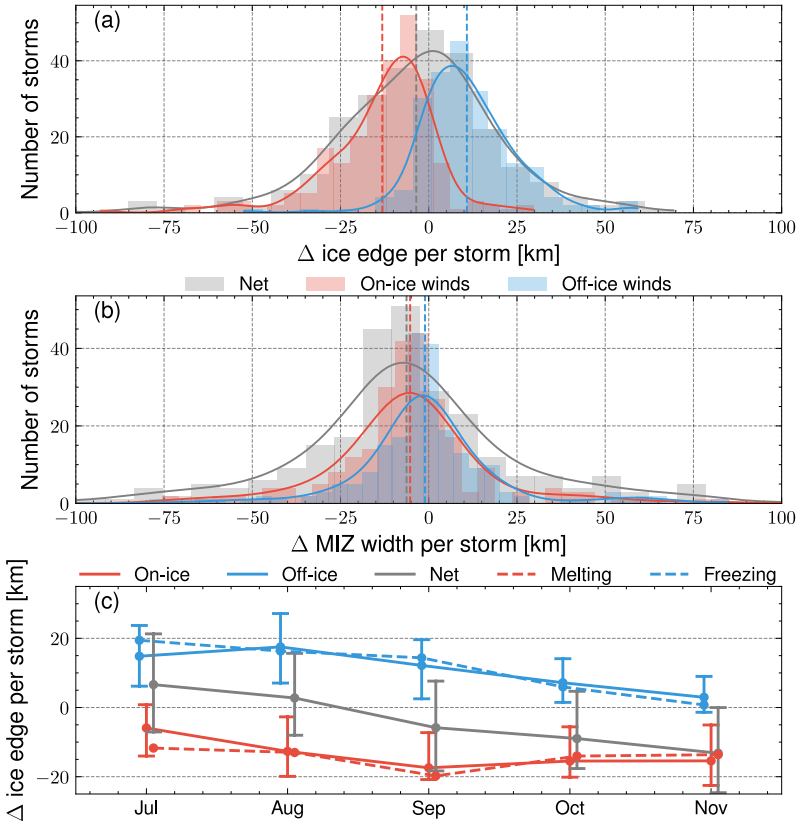

Figure 8. Effect of wind events on ice edge location and MIZ width. Line plots with interquartile ranges for July to November, averaged over 2015–2018, grouped by event type. (a) Change in ice edge location per storm, and (b) change in MIZ width per storm, grouped by on-ice winds (red), off-ice winds (blue), and net change over the cyclone crossing (grey), with their respective means indicated by vertical dashed lines. (c) Seasonal variation in ice edge location change, grouped by on-ice winds (solid red), off-ice winds (solid blue), net change, melting (dashed red), and freezing (dashed blue). Error bars denote interquartile ranges.

4.4 Impacts of Major Wave-Induced Breakup Events on the Antarctic MIZ Width

The criterion for major breakup events is designed to capture floe breakup across the entire ice pack. However, the MIZ only widens if breakup reduces floe sizes at the inner boundary of the MIZ to below 100 m. Figure 10 illustrates the impact of major and minor breakup events on Antarctic MIZ width during cyclones. Histograms display changes in MIZ width grouped by wave-induced breakup events, with the corresponding box plots shown above. During minor breakup events, the MIZ width typically reduces as the breakup is outweighed by other processes, with the median narrowing by approximately 11 km (∼10% of the circumpolar average width). In contrast, major breakup events lead to significant MIZ widening, with a median increase of roughly 31 km (∼25% of the circumpolar average width).

https://doi.org/10.5194/egusphere-2025-5209
Preprint. Discussion started: 11 February 2026

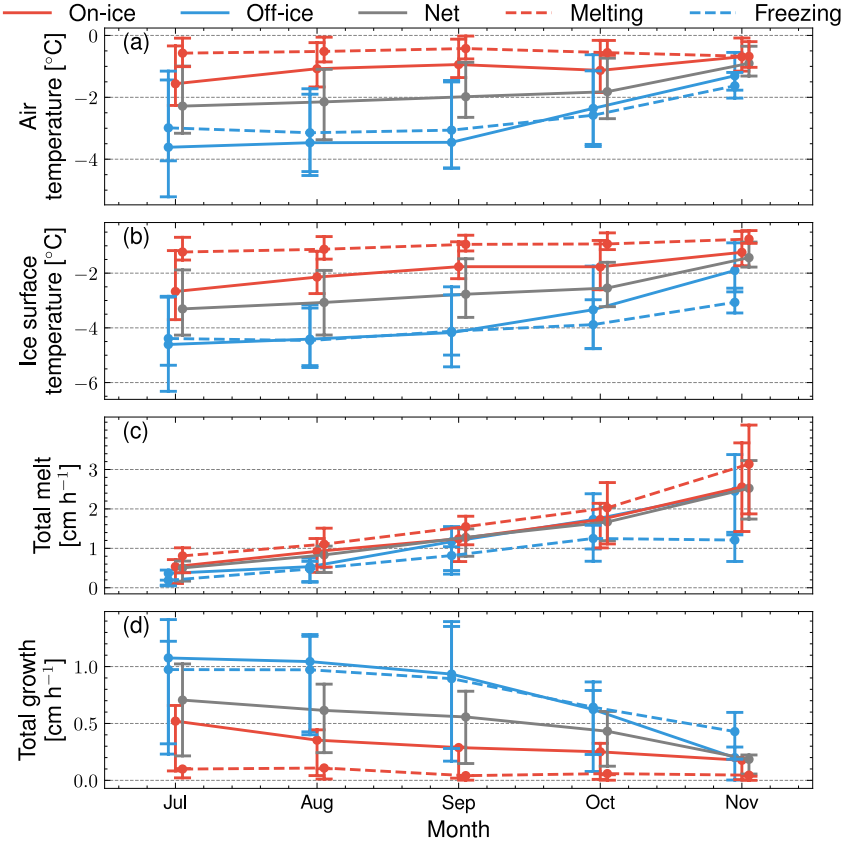

Figure 9. Seasonal thermodynamic impacts of cyclones on the Antarctic MIZ. Line plots with interquartile ranges for July to November, averaged over 2015–2018 and grouped by event type. Panels show (a) air temperature, (b) ice surface temperature, (c) total melt, and (d) total growth. Total melt is the sum of top, lateral, and bottom melt, while total growth includes frazil and congelation production. Note that the y-axis scales in (c) and (d) differ.

Seasonal variability in wave-induced breakup and its effect on MIZ width is shown in Figure 10(b). Major breakup events consistently produce substantial MIZ widening, with the largest impacts in November, coinciding with circumpolar MIZ expansion following earlier narrowing (see Supplemental Material Fig. S1). Minor breakup events, by contrast, generally lead to MIZ narrowing, as reflected in the small interquartile range, with this effect increasing toward November. The net change in MIZ width is defined as the difference before and after cyclone crossings, including cases with no major or minor breakup. During winter, minor breakup events dominate the mean MIZ response, whereas from September to November, when the circumpolar MIZ is relatively narrow, major breakup events become more influential, driving the net change toward zero while increasing variability. In comparison, the ice edge expands during cyclones in mid-winter and retreats later in the season (Fig. 8), indicating that the inner MIZ boundary retreats faster than the ice edge, resulting in MIZ widening.

https://doi.org/10.5194/egusphere-2025-5209
Preprint. Discussion started: 11 February 2026

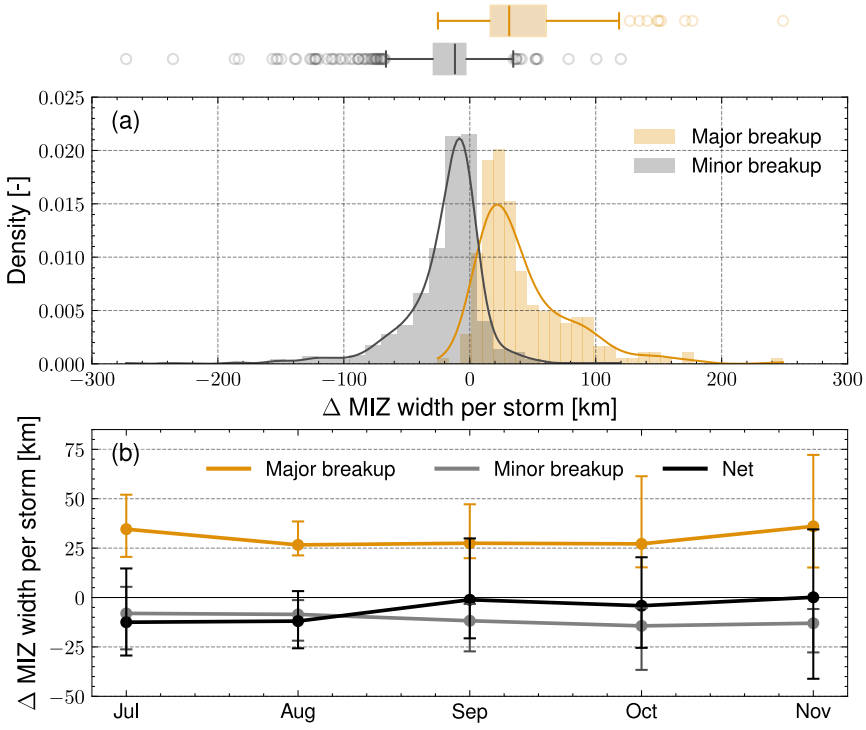

Figure 10. Changes in MIZ width associated with major and minor breakup events. (a) Histograms of the signed change in MIZ width per cyclone, grouped by wave-induced breakup event status. Overlaid are kernel density estimates (solid lines), with corresponding box plots shown above. Each histogram is normalised by event type, and approximately 40% of cyclones experienced at least one major breakup event. (b) Median change in MIZ width per storm from July to November for each breakup event and the net change over a cyclone crossing, with bars indicating the 25th and 75th percentiles.

Since the magnitude of wave-induced breakup depends on wave energy and the distance that waves propagate before encountering floes large enough to fracture, we examine the influence of wave energy and initial MIZ width on the breakup rate. The incident significant wave height, $H_s = 4\sqrt{m_0}$, where m_0 is the variance of sea surface elevation, measured one grid cell north of the ice edge, relates to the total wave energy at that location. The initial MIZ width is defined as the width immediately preceding a major breakup event.

To assess the relationship between wave energy (significant wave height) and initial MIZ width during major breakup events, Figure 11(a) presents the distribution of $H_s^{\max}$ – the maximum significant wave height at the ice edge – plotted against the initial MIZ width. The colour of each data point represents the amount of wave-induced breakup. Since these variables are not necessarily linearly related to breakup rates, quantifying their relative contributions is challenging. To explore how these variables covary with expected breakup severity, we apply a random forest regression, using $H_s^{\max}$ and the initial MIZ width as predictors and the rate of wave-induced breakup as the response variable. A random forest model is selected due to its ability to capture nonlinear relationships through a piecewise constant function (Breiman, 2001). The predicted breakup from the random

https://doi.org/10.5194/egusphere-2025-5209
Preprint. Discussion started: 11 February 2026

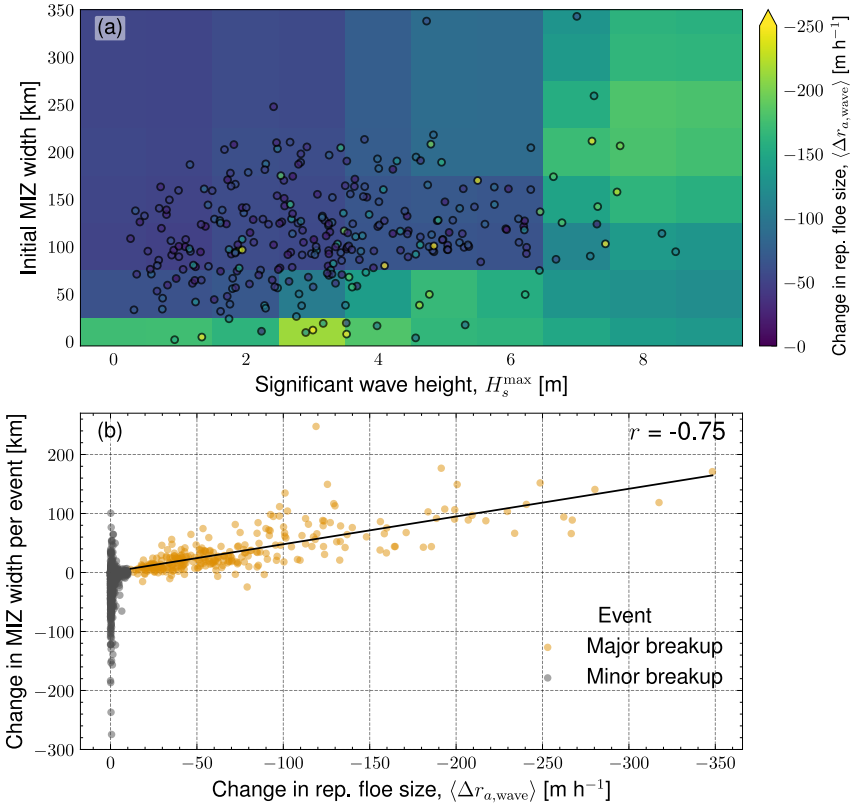

Figure 11. The relationships between MIZ widths and wave heights to wave-induced breakup during major breakup events. (a) Relationship between Antarctic initial MIZ width (taken just before a major breakup event) and the maximum significant wave height during each major breakup event, $H_s^{\max}$. The average wave-induced breakup over the event is shown as coloured dots with the heatmap corresponding to the predicted breakup from a random forest regression trained on initial MIZ width and significant wave height. (b) Change in MIZ width per event versus average wave-induced breakup, grouped by breakup event type. The correlation coefficient for major breakup events is displayed in the top-right corner. Note that the x-axis is inverted.

forest model is represented by the background colour in Figure 11. Narrow MIZs (0–25 km) experience increased breakup, whereas wider MIZs require greater wave energy to trigger breakup. For wave heights exceeding 6 m, breakup becomes more prevalent regardless of the MIZ width for the analysed data range.

We examine how the MIZ width evolves during wave-induced breakup events to investigate where breakup occurs across the ice cover. Figure 11(b) illustrates the MIZ width change for major and minor breakup events. Major breakup events are almost always associated with MIZ widening, with a moderate to strong negative relationship between wave-induced breakup and changes in MIZ width. In contrast, during minor breakup events, small amounts of breakup do not appear to drive MIZ width changes; instead, these changes are likely governed by other factors (e.g., winds and thermodynamics). This result suggests that fracturing occurs primarily along the inner boundary of the MIZ during major breakup events.

https://doi.org/10.5194/egusphere-2025-5209
Preprint. Discussion started: 11 February 2026

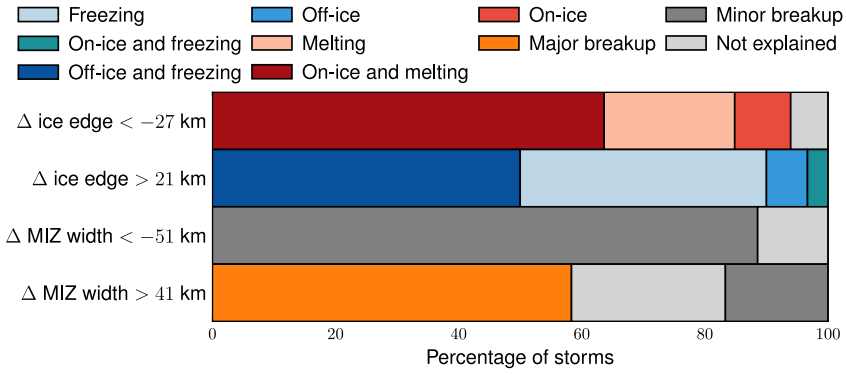

Figure 12. Likelihood of each event occurring during extreme changes in ice edge position and MIZ width. Extreme changes are defined as values below the 10th percentile or above the 90th percentile, with corresponding thresholds displayed on the vertical axis. If the contribution of one or more events is within 10% of the total modelled change, all contributing events are recorded. "No event" indicates cases where none of the events explain at least 70% of the total change.

4.5 Extreme Changes in the Ice Edge Location and MIZ Width

To examine extreme cases driven by wind, thermodynamic, and wave events, we now analyse cyclones exceeding the 10th and 90th percentiles of change in the ice edge location or MIZ width (Fig. 12). This approach isolates the contributions of extreme changes to ice edge compaction or expansion and MIZ width changes, which still occur over short time periods. As winds and thermodynamics primarily govern processes at the ice edge, while waves influence the inner MIZ boundary (§4.3 and §4.4), we analyse these effects separately. When multiple processes contribute to observed changes, they are grouped into joint classifications (e.g., "on-ice and melting"). Light grey shading in Figure 12 indicates changes that are not captured by our event classification.

When the ice edge retreats by at least 27 km during a storm, most cases (64 %) result from the combined effects of on-ice winds and melting, while 30 % are driven by either factor alone. Extreme ice edge expansion is primarily driven by off-ice winds and freezing, accounting for half of the cases; freezing alone explains 40 %, indicating that expansion events nearly always occur under freezing conditions. Expansion events, however, are smaller in magnitude than compaction events (21 km versus −27 km).

Extreme MIZ narrowing coincides with minor breakup events in 88% of cases, emphasising that processes other than wave-induced breakup likely cause these changes. In contrast, MIZ widening is often associated with major breakup events (58% of the cases), indicating that such events drive extreme widening of the MIZ. However, the event categorisation does not account for all extreme changes, as some minor breakup events also occur during periods of extreme MIZ widening. These findings suggest that wave-induced breakup – or the absence thereof – is a strong indicator of extreme MIZ change: widening under energetic wave conditions and narrowing under low wave activity. The remaining extreme events show no clear association

https://doi.org/10.5194/egusphere-2025-5209
Preprint. Discussion started: 11 February 2026

with either major or minor breakup, possibly because some wave impacts were short-lived and failed to meet the six-hour threshold, or because other processes such as wind-driven drift and thermodynamic effects dominate the response.

5 Conclusions and Discussion

We used the CICE6 sea ice model with a wave–ice propagation module at 0.25° resolution to analyse changes in Antarctic MIZ width and ice edge location in response to extratropical polar cyclone crossings. Across 396 cyclone events over predominantly winter months (July to November) 2015–2018, we examined hourly variations in winds, thermodynamics, and wave processes, enabling a novel assessment of their combined influence on the Antarctic ice cover. As cyclones approach the winter MIZ, on-ice winds heat the ice surface, often exceeding its melting point, but once cyclones leave the the MIZ off-ice winds drive rapid cooling and ice-edge advance (Figs. 5–7). Wave-induced breakup events can coincide with melting or freezing, thereby adding complexity to understanding the changing MIZ width. The ice edge is primarily sensitive to melting and freezing, whereas breakup events largely control the interior MIZ boundary. By decomposing the MIZ width into these boundaries, we quantified the contributions of each of these processes.

The classification of thermodynamic and wind events revealed positive and negative changes in the ice edge during cyclone crossings of the MIZ (Fig. 8). The predominance of melt over growth was expected, given that the main months of ice growth were excluded and Antarctic sea ice thermodynamics are known to be asymmetric (Roach et al., 2023). Nevertheless, the net impact of cyclone crossings was found to be strongly seasonal: frequent off-ice winds and freezing temperatures in July caused a slight ice-edge advance, whereas on-ice winds and melting temperatures by November led to a net retreat. Despite this trend, melting events frequently occurred throughout winter, suppressing sea ice growth during cyclones (Fig. 6), consistent with satellite data derived findings (e.g., Kimura et al., 2022).

Extreme events generally caused ice-edge retreat, with on-ice winds and ice melt acting in concert (Fig.12). Ice-edge advances were more variable, often driven by freezing temperatures. Overall, thermodynamics was found to play a dominant role in these extreme cases. Coupling to a full ocean model, rather than a the mixed-layer parameterisation used in this study, would more accurately represent heat exchanges between the atmosphere, sea ice, and the ocean surface, and, hence, better capture the sources of the temperature changes. The absence of heat (and momentum) fluxes from the ocean limits our analysis to short-term impacts, as we cannot account for ocean–atmosphere fluxes that may influence subsequent ice growth (Smith et al., 2018), upper-ocean mixing, or even storm activity (Josey et al., 2024).

Waves are proposed to play a key role in modifying MIZ widths during cyclone crossings (Vichi et al., 2019). One of the presented case studies (§3.3) demonstrated the potential for rapid MIZ widening ($\sim$90 km over 12 hours) due to wave-induced breakup of previously consolidated ice. Statistically, these "major breakup events" were found to occur in 40% of the tracked cyclones and widen the MIZ by $\sim$30 km on average. Major breakup was most common in narrow MIZs ($<$ 50 km) or under large wave conditions (maximum $H_s > 6$ m), producing further breakup in MIZs that are already hundreds of kilometres in width. Breakup events at these distances from the ice edge have been observed in the field (Kohout et al., 2016), and our

https://doi.org/10.5194/egusphere-2025-5209
Preprint. Discussion started: 11 February 2026

findings provide additional evidence for wave–ice interactions rapidly widening the MIZ during cyclone crossings, as suggested by Vichi et al. (2019).

Discrepancies between the atmospheric forcings used for the wave hindcast and that used in CICE6-WIM introduce uncertainty in how winds correlate with wave activity. Consequently, we did not analyse a direct causal link between cyclones and local wave generation – since the wave hindcast includes swell from the far field – but instead examined how ice cover evolves when cyclones coincide with wave-driven breakup events. Coupling to a wave model would allow for consistency in atmospheric forcing as well as the generation and directional propagation of wave energy by cyclones during their passage over the MIZ (Alberello et al., 2022; Cooper et al., 2022), thereby alleviating this limitation. However, recent evidence suggests that the current breakup parameterisation (Horvat and Tziperman, 2015) may produce unrealistically small floes when wind waves propagate within the ice cover (Cooper et al., 2022). Since modelled floe sizes increase sharply over the transition from MIZ to pack ice (Fig. 4), capturing the feedbacks between waves and floe size may require subgrid-scale representations of wave attenuation and breakup (e.g., Bennetts et al., 2015). Because the ice edge largely determines where wave attenuation begins, future work should prioritise implementing wave–ice processes that influence this location, such as wave radiation stress or wave-induced ocean mixing (Dumont, 2022; Boutin et al., 2022; Thomas et al., 2019).

In conclusion, extratropical cyclones were found to cause rapid changes (over hours to days) in the location and width of the Antarctic MIZ, consistent with observations (Vichi et al., 2019). Thermodynamic processes emerged as key drivers of the outer MIZ boundary (ice edge), operating through both synoptic weather systems and seasonal cycles. Wave activity was found to govern changes in MIZ width, underscoring the importance of explicitly representing wave–ice interactions in climate models (Bennetts et al., 2022b). Future work should focus on coupling global sea ice and wave models to assess whether cyclone-driven processes enhance or suppress local sea ice production (Smith et al., 2018), how storms contribute to Antarctic sea ice extent anomalies (e.g., in 2023; Josey et al., 2024), and whether such events intensify subsequent storms (Zhang et al., 2024).

Code and data availability. The code to reproduce the figures in the manuscript are publicly available at: https://github.com/NoahDay/Day2025-MIZ-cyclones. The data used in this manuscript is publicly available at: https://zenodo.org/records/16251054 (Day, 2025). The cyclone track dataset of Phillips (2020) is governed by the NERC data policy http://www.nerc.ac.uk/research/sites/data/policy/ and supplied under Open Government Licence v3 http://www.nationalarchives.gov.uk/doc/open-government-licence/version/3/.

Appendix A: Forcing Data Consistency Tests

Consistency tests are performed to assess differences between two reanalysis products: JRA55-do (Tsujino et al., 2018) (used to force CICE6–WIM) and Climate Forecast System version 2 (CFSv2; Saha et al., 2014) (used to force the wave hindcast that drives the WIM). Analysis focuses on three key atmospheric fields: sea level pressure, and the 10-m zonal (u) and meridional (v) wind components. Comparisons for the three selected case studies are shown in Figures A1–A3.

https://doi.org/10.5194/egusphere-2025-5209
Preprint. Discussion started: 11 February 2026

Figure A1(a–c) presents mean sea level pressure fields from the JRA55 reanalysis over 250–290° E from 2–9 August, consistent with the spatio-temporal domain defined in §3.1. Figure A1(d–f) shows the corresponding fields from the CFSv2 reanalysis. Minor differences in isobar structure are apparent between the datasets, but both capture the low-pressure system associated with the cyclone, exhibiting similar trajectories consistent with cyclone tracks derived from ERA-Interim (Keay et al., 2020; Dee et al., 2011). Time series at the location where the cyclone first intersects the ice edge (Fig. A1g–i) show strong agreement in sea level pressure across the reanalyses, with a distinct minimum coinciding with the cyclone's passage (marked by a magenta dot). The u- and v-components of wind display moderate agreement; however, both indicate a similar qualitative transition from westerly–northerly winds prior to crossing, to easterly–southerly winds post-crossing. Some discrepancies are attributable to differences in spatial and temporal resolution between JRA55-do and CFSv2, which are provided on different grids.

Similar patterns to those shown in Figure A1 are evident in the other case studies presented in Figures A2 and A3, demonstrating a level of consistency between the atmospheric reanalyses used. In general, the comparison reveals a high degree of agreement in sea level pressure across the datasets, while wind components show moderate consistency, supporting the robustness of the atmospheric forcing across case studies.

Appendix B: MIZ Width Quantification

Day et al. (2024) give evidence that a k-means classification of sea-ice variables provides an effective estimate of the Antarctic MIZ width, including strong correspondence with waves-in-ice remote sensing. Because the model outputs in this study are restricted to winter and spring, the resulting k-means-derived MIZ is seasonally biassed due to incomplete sampling of the state space. Thus, we adopt a simplified definition based on a representative floe-size threshold (Figure B1), which provides an interpretable diagnostic of the wave-induced breakup processes analysed in our study.

Appendix C: Time Series from Case Studies

Figures C1-–C3 show time series of key forcing and modelled sea-ice variables for the three case studies in Section 3. All time series are sampled along the modelled 15% ice edge, providing a detailed view of how cyclone-related forcing influences the evolving sea-ice state. The left column presents surface air pressure and wind components, the middle column shows sea surface temperature, sea-ice concentration and significant wave height, and the right column displays sea-ice thickness, ice age and representative floe size.

The first case study highlights the role of thermodynamic processes during a cyclone crossing the Antarctic MIZ. In this case, the cyclone rapidly deepens as it approaches the ice edge, reaching its minimum central pressure at the point of crossing (Fig. C1a). This intensification coincides with a pulse of increased sea surface temperature (Fig. C1b). Evidence of substantial new ice formation is apparent, marked by an increase in sea ice concentration, a corresponding drop in sea surface temperature, and a decrease in sea ice age (Fig. C1b,e,i). In this case, the sea ice remains thin, with thickness around 0.15 m throughout

https://doi.org/10.5194/egusphere-2025-5209
Preprint. Discussion started: 11 February 2026

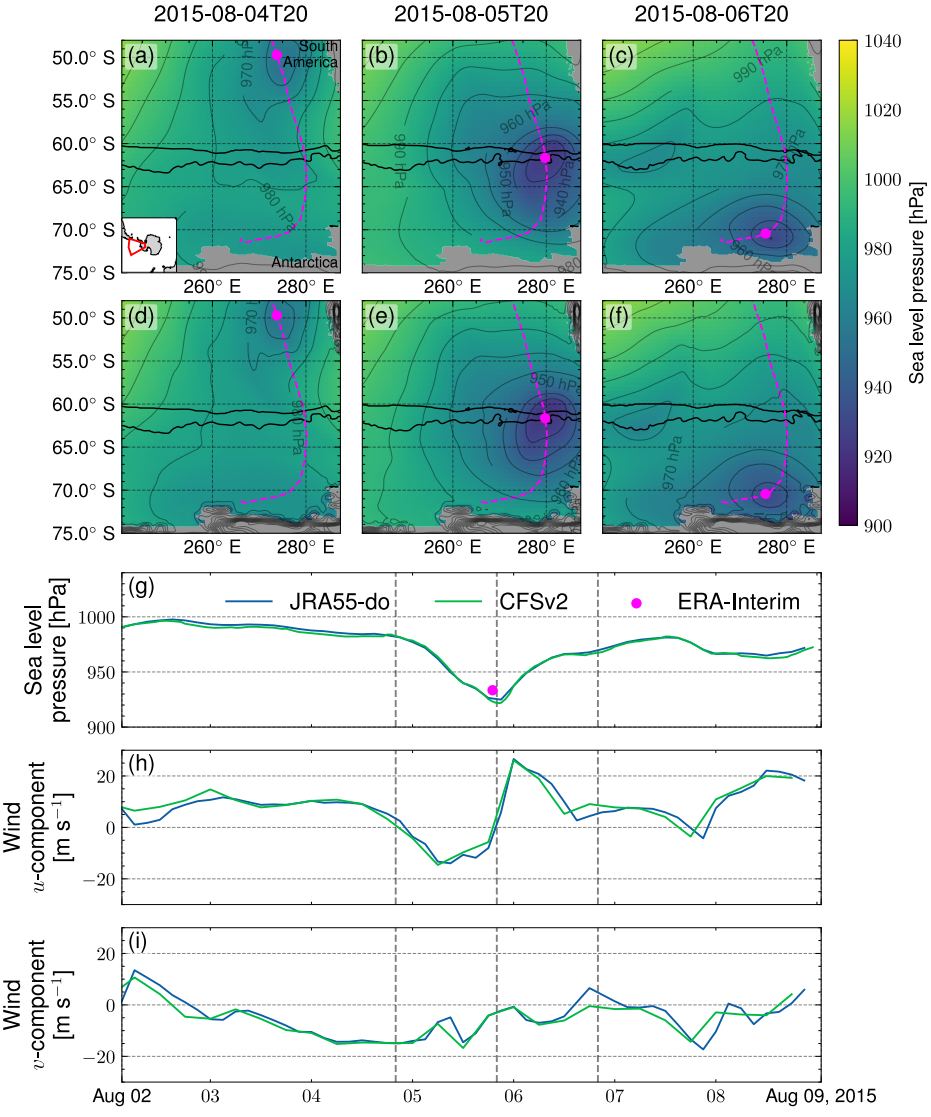

Figure A1. Comparison of atmospheric forcing datasets at ∼ 280° E from 2–9 August, 2015. (a–c) Sea level pressure from JRA55-do: (a) 24 hours before the cyclone's crossing; (b) at the time of crossing; and (c) 24 hours after. Isobars are overlaid in 10 hPa intervals, along with the cyclone's location (magenta dot) and its track (dashed magenta line). Black contours indicate the boundaries of the MIZ. (d–f) As in (a–c), but using Climate Forecast System version 2 (CFSv2). (g–i) Time series at the cyclone crossing location (magenta dot in panels b and e) of: (g) sea level pressure, (h) wind u-component, and (i) wind v-component. Time series for JRA55-do and CFSv2 are shown in blue and green, respectively. The sea level pressure from the ERA-Interim cyclone track is also shown in panel (g).

the event. Winds are dominated by the zonal (u) component (Fig. C1d), meaning the north–south changes of the ice edge are

https://doi.org/10.5194/egusphere-2025-5209
Preprint. Discussion started: 11 February 2026

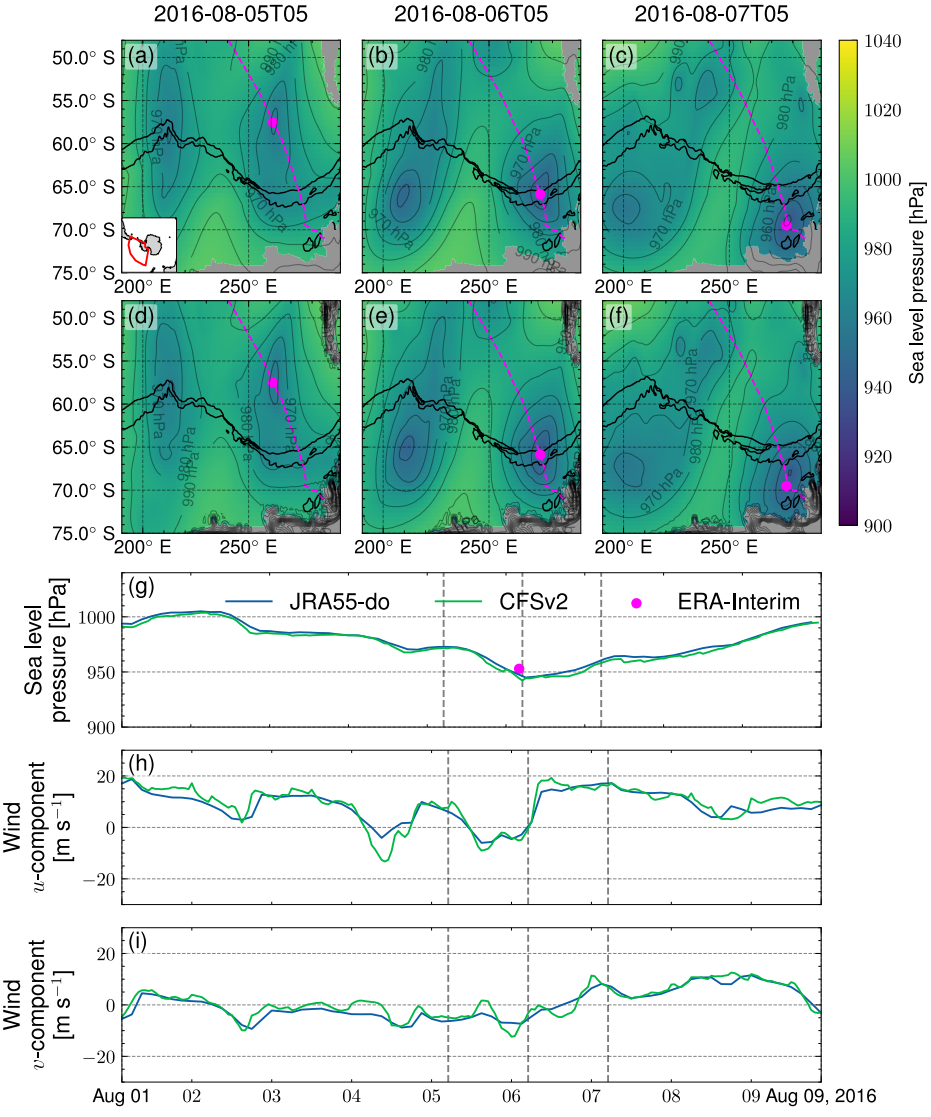

Figure A2. Same as Figure A1 but at ∼ 270° E from 2–9 August, 2016.

limited. These conditions suggest that thermodynamic processes were the dominant factor that influenced the sea ice response during this cyclone.

Cyclone-induced sea ice drift is much more pronounced in the second case study shown in Figure C2. Again, the cyclone drops to a minimum pressure at the ice edge, however, in this case, sea ice concentration is high (Fig. C2e) and relatively thick (∼0.8 m; Fig. C2c), insulating the sea surface (Fig. C2b). The meridonal wind component (v) increases from approximately -5 to 5 m s^{-1} (Fig. C2e) as the storm passes, promoting a northward advance of the ice edge. The advancement contributes to new ice formation, as indicated by the cooling of the sea surface and decreases in sea ice thickness and age (Fig. C2b,c,i).

https://doi.org/10.5194/egusphere-2025-5209
Preprint. Discussion started: 11 February 2026

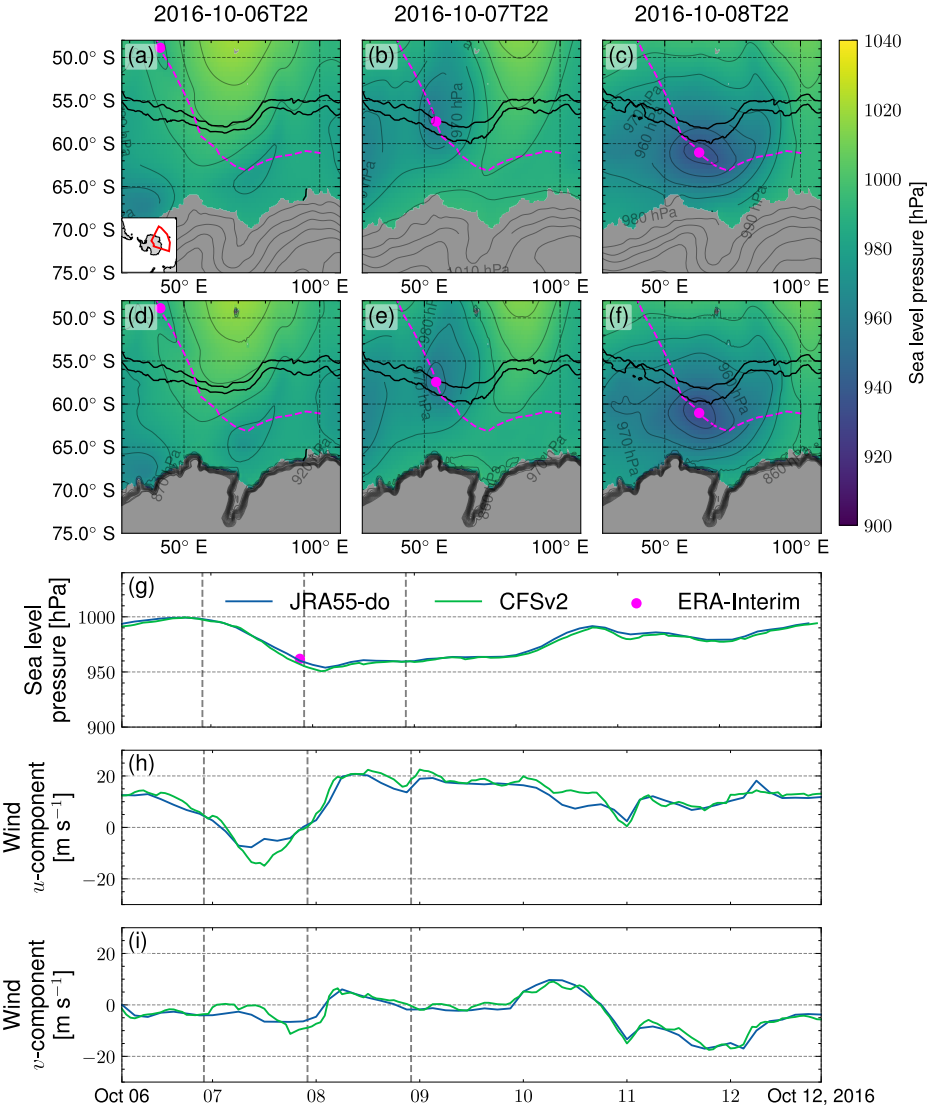

Figure A3. Same as Figure A1 but at $\sim 50^\circ$ E from 6–10 October, 2016.

The third case study contrasts with the previous two. Surface pressure decreases are more sustained, indicative of a relatively large cyclone compared to the earlier events. The sea ice remains relatively mature (approximately 100 days old) and moderately thick (~ 0.35 m). Wave activity is substantially greater, with wave heights exceeding 4 m (averaged over the MIZ), compared to 0.5–1 m in the preceding cases. The larger waves restrict floe sizes, although periods of wave subsidence permit the formation of larger floes (Fig. C3f). There is little evidence of significant melting or freezing, as indicated by minimal changes in sea ice age (Fig. C3f). Instead, changes in sea ice concentration appear to be driven by zonal transport (Fig. C3d).

https://doi.org/10.5194/egusphere-2025-5209
Preprint. Discussion started: 11 February 2026

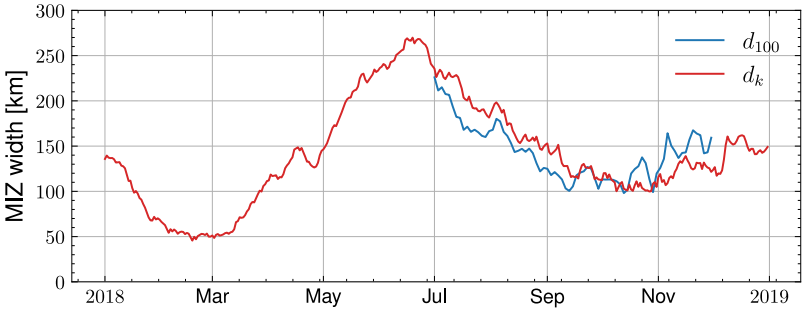

Figure B1. Comparison of Antarctic MIZ widths derived from k-means analysis on 1° CICE6-WIM daily outputs (red line) and a representative floe size (r_a) threshold of 100 m applied to 0.25° CICE6-WIM hourly outputs (blue line) for 2018.

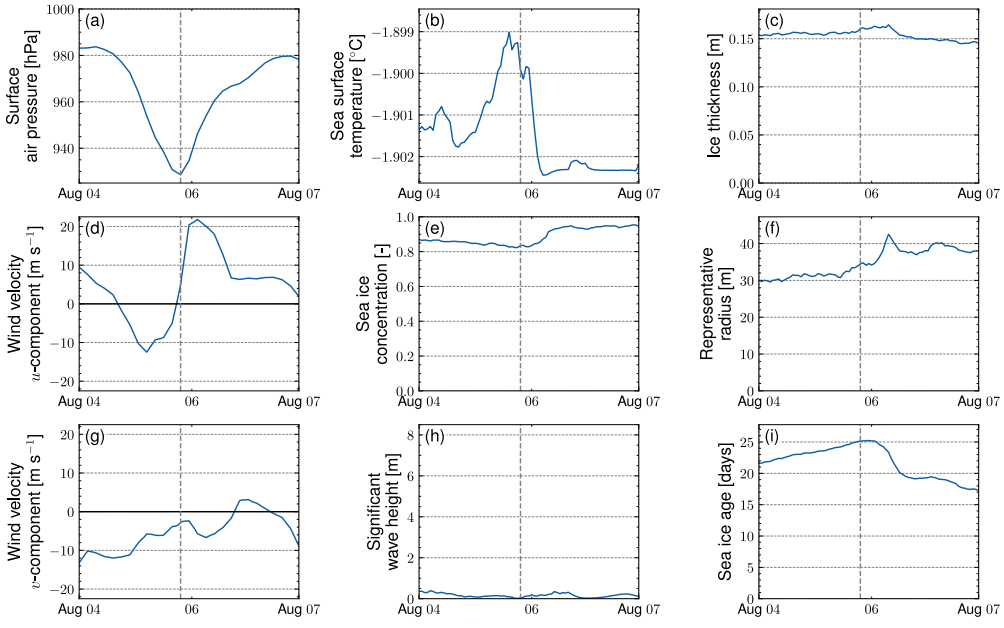

Figure C1. Time series from the ice edge taken during the case study in §3.1 (a) Surface air pressure; (b) sea surface temperature; (c) u-component of wind velocity; (d) sea ice concentration; (e) v-component of wind velocity; (f) sea ice age; (g) significant wave height; (h) representative floe size. The time at which the cyclone crosses the ice edge is shown as grey-dashed vertical lines.

https://doi.org/10.5194/egusphere-2025-5209
Preprint. Discussion started: 11 February 2026

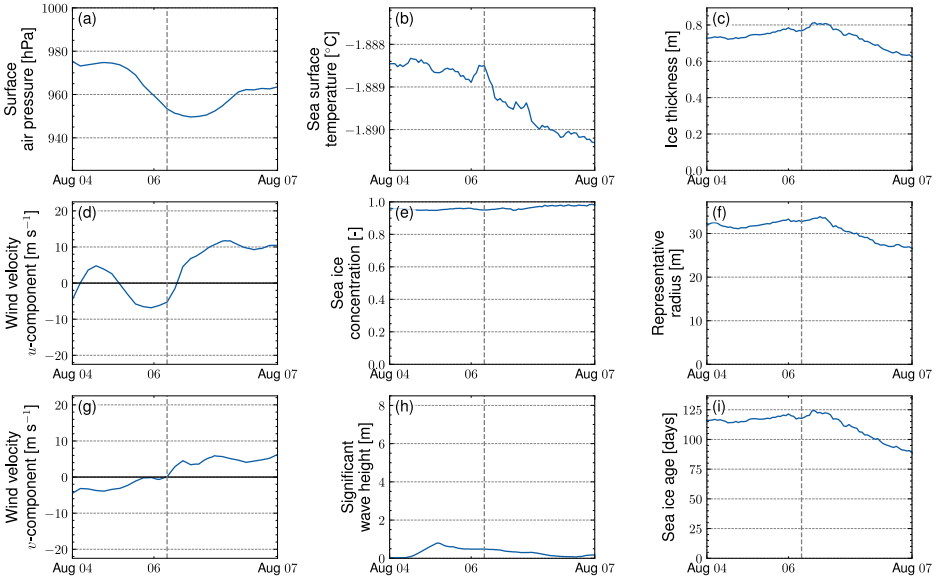

Figure C2. As in Figure C1, but for the case study in §3.2.

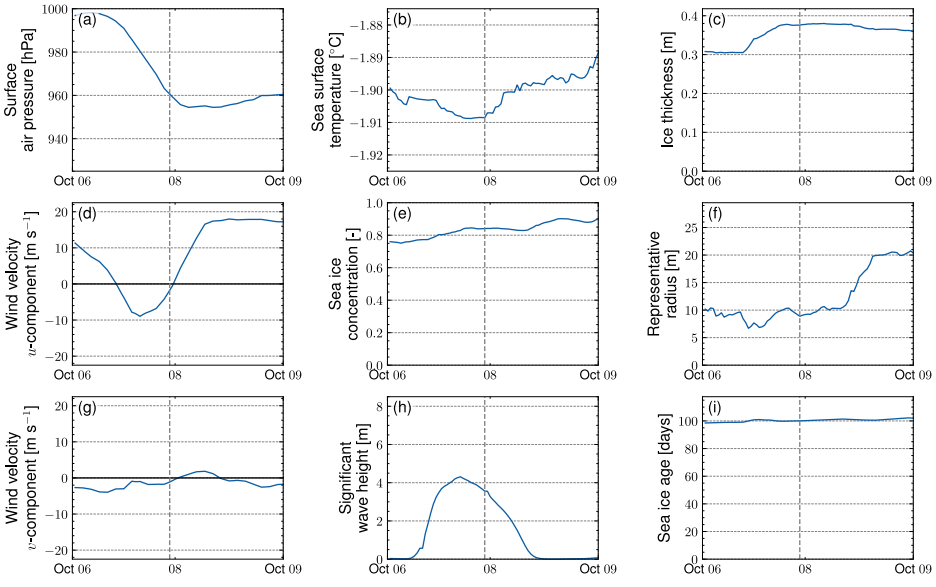

Figure C3. As in Figure C1, but for the case study in §3.3.

Appendix D: Oceanic Contribution

The propensity for sea ice to melt or freeze within CICE is determined by the freeze/melt potential, F_{frzmlt}, which is calculated as (Hunke et al., 2021)

$$F_{\text{frzmlt}} = \frac{1}{\Delta t}(T_f - T_{\text{SST}})c_p\rho_w h_{\text{mix}} \tag{D1}$$

https://doi.org/10.5194/egusphere-2025-5209
Preprint. Discussion started: 11 February 2026

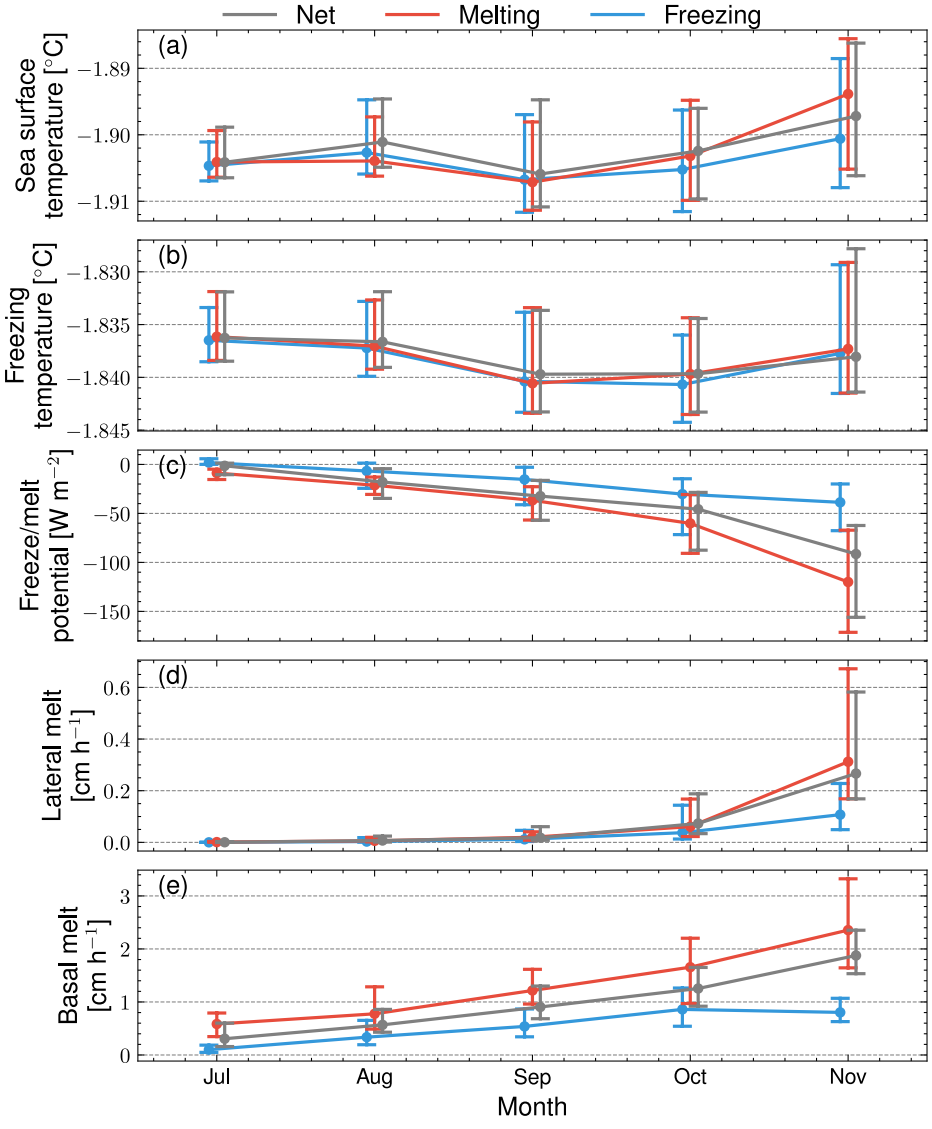

Figure D1. Oceanic contributions to sea ice melt during cyclones crossing the Antarctic MIZ. Line plots (medians) with interquartile ranges for July to November, averaged over 2015–2018 and grouped by event type (note that wind events are not included to reduce clutter). Panels show (a) sea surface temperature, (b) freezing temperature, (c) freeze/melt potential, (d) lateral melt, and (e) basal melt. A negative freeze/melt potential will promote ice melting whereas a positive promotes new ice formation.

where Δt is the model timestep, T_{SST} is sea surface temperature, c_p =4,218 J kg^{-1} K^{-1} is ocean heat capacity, ρ_w =1,026 kg m^{-3} is ocean water density, and $h_{\mathrm{mix}} = 20$ m is the mixed-layer depth.

Figure D1 illustrates seasonal changes in (a) sea surface temperature (SST), (b) sea ice freezing temperature (T_f), (c) freeze/melt potential, (d) lateral melt rate, and (e) basal melt rate. As the season progresses toward summer, SST increases

https://doi.org/10.5194/egusphere-2025-5209
Preprint. Discussion started: 11 February 2026

more rapidly than T_f, leading to a greater temperature difference and a corresponding increase in melt potential from the ocean (i.e., a more negative freeze/melt potential; see Eq. D1). The enhanced melting potential is reflected in increases in both lateral and basal melt rates, with basal melt generally dominating, although lateral melt remains a non-negligible contributor. Notably, melt events—defined here based on the surface temperature of sea ice—are primarily driven by basal melt, suggesting that the elevated air and surface ice temperatures associated with cyclones may also act to warm the underlying ocean.

Author contributions. All authors conceptualised the study, designed the methodology, as well as reviewed and edited the manuscript. NSD and LGB prepared the original draft. NSD performed the data curation, formal analysis, investigation, validation, visualisation. LGB completed funding acquisition, and project administration. LGB and SPO supervised the project.

Competing interests. The contact author has declared that none of the authors have any competing interests.

Acknowledgements. NSD and LGB are supported by Australian Research Council grants DP240100325, FT190100404 and SR20010000. NSD was supported by the Consortium for Ocean-Sea Ice Modelling in Australia (COSIMA). The authors would like to thank the Australian Government funded National Research Infrastructure (NCI) for the computational facilities to conduct these simulations (projects `ia40` and `ps29`) as well as for the continued hosting of the data by the Australian Antarctic Partnership Program (AAPP) (project `gv90`).

https://doi.org/10.5194/egusphere-2025-5209
Preprint. Discussion started: 11 February 2026

References

Alberello, A., Onorato, M., Bennetts, L. G., Vichi, M., Eayrs, C., MacHutchon, K., and Toffoli, A.: Pancake ice floe size distribution during the winter expansion of the Antarctic marginal ice zone, The Cryosphere, 13, 41–48, https://doi.org/10.5194/tc-13-41-2019, 2019.

Alberello, A., Bennetts, L. G., Heil, P., Eayrs, C., Vichi, M., MacHutchon, K., Onorato, M., and Toffoli, A.: Drift of pancake ice floes in the winter Antarctic marginal ice zone during polar cyclones, J. Geophys. Res. Oceans, 125, e2019JC015 418, https://doi.org/10.1029/2019JC015418, 2020.

Alberello, A., Bennetts, L. G., Onorato, M., Vichi, M., MacHutchon, K., Eayrs, C., Ntamba, B. N., Benetazzo, A., Bergamasco, F., Nelli, F., Pattani, R., Clarke, H., Tersigni, I., and Toffoli, A.: Three-dimensional imaging of waves and floes in the marginal ice zone during a cyclone, Nat. Commun., 13, 4590, https://doi.org/10.1038/s41467-022-32036-2, 2022.

Asplin, M. G., Scharien, R., Else, B., Howell, S., Barber, D. G., Papakyriakou, T., and Prinsenberg, S.: Implications of fractured Arctic perennial ice cover on thermodynamic and dynamic sea ice processes, J. Geophys. Res. Oceans, 119, 2327–2343, https://doi.org/10.1002/2013JC009557, 2014.

Bennetts, L. G.: Waves in ice, in: Reference Module in Earth Systems and Environmental Sciences, Elsevier, https://doi.org/10.1016/B978-0-323-85242-5.00037-3, 2025.

Bennetts, L. G., O'Farrell, S., Uotila, P., and Squire, V. A.: An idealized wave–ice interaction model without subgrid spatial or temporal discretizations, Ann. Glaciol., 56, 258–262, https://doi.org/10.3189/2015AoG69A599, 2015.

Bennetts, L. G., O'Farrell, S., and Uotila, P.: Impacts of ocean-wave-induced breakup of Antarctic sea ice via thermodynamics in a stand-alone version of the CICE sea-ice model, The Cryosphere, 11, 1035–1040, https://doi.org/10.5194/tc-11-1035-2017, 2017.

Bennetts, L. G., Bitz, C. M., Feltham, D. L., Kohout, A. L., and Meylan, M. H.: Theory, modelling and observations of marginal ice zone dynamics: multidisciplinary perspectives and outlooks, Philos. Trans. R. Soc. A, 380, 20210 265, https://doi.org/10.1098/rsta.2021.0265, 2022a.

Bennetts, L. G., Bitz, C. M., Feltham, D. L., Kohout, A. L., and Meylan, M. H.: Marginal ice zone dynamics: future research perspectives and pathways, Philos. Trans. R. Soc. A, 380, 20210 267, https://doi.org/10.1098/rsta.2021.0267, 2022b.

Bennetts, L. G., Shakespeare, C. J., Vreugdenhil, C. A., Foppert, A., Gayen, B., Meyer, A., Morrison, A. K., Padman, L., Phillips, H. E., Stevens, C. L., Toffoli, A., Constantinou, N. C., Cusack, J. M., Cyriac, A., Doddridge, E. W., England, M. H., Evans, D. G., Heil, P., Hogg, A. M., Holmes, R. M., Huneke, W. G. C., Jones, N. L., Keating, S. R., Kiss, A. E., Kraitzman, N., Malyarenko, A., McConnochie, C. D., Meucci, A., Montiel, F., Neme, J., Nikurashin, M., Patel, R. S., Peng, J.-P., Rayson, M., Rosevear, M. G., Sohail, T., Spence, P., and Stanley, G. J.: Closing the loops on Southern Ocean dynamics: from the circumpolar current to ice shelves and from bottom mixing to surface waves, Reviews of Geophysics, 62, e2022RG000 781, https://doi.org/10.1029/2022RG000781, 2024.

Blanchard-Wrigglesworth, E., Donohoe, A., Roach, L. A., DuVivier, A., and Bitz, C. M.: High-frequency sea ice variability in observations and models, Geophys. Res. Lett., 48, e2020GL092 356, https://doi.org/10.1029/2020GL092356, 2021.

Blanchard-Wrigglesworth, E., Webster, M., Boisvert, L., Parker, C., and Horvat, C.: Record Arctic cyclone of January 2022: characteristics, impacts, and predictability, Journal of Geophysical Research: Atmospheres, 127, e2022JD037 161, https://doi.org/10.1029/2022JD037161, 2022.

Boutin, G., Williams, T., Horvat, C., and Brodeau, L.: Modelling the Arctic wave-affected marginal ice zone: a comparison with ICESat-2 observations, Philos. Trans. R. Soc. A, 380, 20210 262, https://doi.org/10.1098/rsta.2021.0262, 2022.

Breiman, L.: Random Forests, Machine Learning, 45, 5–32, https://doi.org/10.1023/A:1010933404324, 2001.

https://doi.org/10.5194/egusphere-2025-5209
Preprint. Discussion started: 11 February 2026

Bretschneider, C. L.: Wave variability and wave spectra for wind-generated gravity waves, Beach Erosion Board, Corps of Engineers, United States, 1959.

Brouwer, J., Fraser, A. D., Murphy, D. J., Wongpan, P., Alberello, A., Kohout, A., Horvat, C., Wotherspoon, S., Massom, R. A., Cartwright, J., and Williams, G. D.: Altimetric observation of wave attenuation through the Antarctic marginal ice zone using ICESat-2, The Cryosphere, 16, 2325–2353, https://doi.org/10.5194/tc-16-2325-2022, 2022.

Brümmer, B., Schröder, D., Müller, G., Spreen, G., Jahnke-Bornemann, A., and Launiainen, J.: Impact of a Fram Strait cyclone on ice edge, drift, divergence, and concentration: possibilities and limits of an observational analysis, J. Geophys. Res. Oceans, 113, https://doi.org/10.1029/2007JC004149, 2008.

Clancy, R., Bitz, C. M., Blanchard-Wrigglesworth, E., McGraw, M. C., and Cavallo, S. M.: A cyclone-centered perspective on the drivers of asymmetric patterns in the atmosphere and sea ice during Arctic cyclones, J. Clim., pp. 1–47, https://doi.org/10.1175/JCLI-D-21-0093.1, 2021.

Cooper, V. T., Roach, L. A., Thomson, J., Brenner, S. D., Smith, M. M., Meylan, M. H., and Bitz, C. M.: Wind waves in sea ice of the western Arctic and a global coupled wave-ice model, Philos. Trans. R. Soc. A, 380, 20210 258, https://doi.org/doi.org/10.1098/rsta.2021.0258, 2022.

Day, N.: Model output: CICE6-WIM 0.25-degree Antarctic sea ice data in response to cyclone activity, https://doi.org/10.5281/zenodo.16251054, 2025.

Day, N. S., Bennetts, L. G., O'Farrell, S. P., Alberello, A., and Montiel, F.: Analysis of the Antarctic marginal ice zone based on unsupervised classification of standalone sea ice model data, J. Geophys. Res. Oceans, 129, e2024JC020 953, https://doi.org/10.1029/2024JC020953, 2024.

de Jager, W. and Vichi, M.: Rotational drift in Antarctic sea ice: pronounced cyclonic features and differences between data products, The Cryosphere, 16, 925–940, https://doi.org/10.5194/tc-16-925-2022, 2022.

Dee, D. P., Uppala, S. M., Simmons, A. J., Berrisford, P., Poli, P., Kobayashi, S., Andrae, U., Balmaseda, M. A., Balsamo, G., Bauer, P., Bechtold, P., Beljaars, A. C. M., Van De Berg, L., Bidlot, J., Bormann, N., Delsol, C., Dragani, R., Fuentes, M., Geer, A. J., Haimberger, L., Healy, S. B., Hersbach, H., Hólm, E. V., Isaksen, L., Kållberg, P., Köhler, M., Matricardi, M., McNally, A. P., Monge-Sanz, B. M., Morcrette, J.-J., Park, B.-K., Peubey, C., De Rosnay, P., Tavolato, C., Thépaut, J.-N., and Vitart, F.: The ERA-Interim reanalysis: configuration and performance of the data assimilation system, Quarterly Journal of the Royal Meteorological Society, 137, 553–597, https://doi.org/10.1002/qj.828, 2011.

Doble, M. J. and Bidlot, J.-R.: Wave buoy measurements at the Antarctic sea ice edge compared with an enhanced ECMWF WAM: progress towards global waves-in-ice modelling, Ocean Modelling, 70, 166–173, https://doi.org/10.1016/j.ocemod.2013.05.012, 2013.

Dumont, D.: Marginal ice zone dynamics: history, definitions and research perspectives, Philos. Trans. R. Soc. A, 380, 20210 253, https://doi.org/10.1098/rsta.2021.0253, 2022.

Eayrs, C., Holland, D., Francis, D., Wagner, T., Kumar, R., and Li, X.: Understanding the seasonal cycle of Antarctic sea ice rxtent in the context of longer-term variability, Reviews of Geophysics, 57, 1037–1064, https://doi.org/10.1029/2018RG000631, 2019.

Finocchio, P. M., Doyle, J. D., Stern, D. P., and Fearon, M. G.: Short-term impacts of Arctic summer cyclones on sea ice extent in the marginal ice zone, Geophys. Res. Lett., 47, https://doi.org/10.1029/2020GL088338, 2020.

Fraser, A. D., Day, N. S., Wang, Z., Bennetts, L. G., Liu, Q., O'Farrell, S., Coleman, R., Voermans, J., Xu, S., Zhu, W., Auger, M., Massom, R. A., Wongpan, P., Craw, L., Brouwer, J., Toyota, T., Heil, P., and Horvat, C.: Revealing the Antarctic marginal ice zone: a decade-long wave-in-ice climatology, In review, 2025.

https://doi.org/10.5194/egusphere-2025-5209
Preprint. Discussion started: 11 February 2026

Golden, K. M., Bennetts, L. G., Cherkaev, E., Eisenman, I., Feltham, D., Horvat, C., Hunke, E., Jones, C., Perovich, D. K., Ponte-Castaneda, P., et al.: Modeling sea ice, Notices of the American Mathematical Society, 67, 1535–1555, 2020.

Graham, R. M., Itkin, P., Meyer, A., Sundfjord, A., Spreen, G., Smedsrud, L. H., Liston, G. E., Cheng, B., Cohen, L., Divine, D., Fer, I., Fransson, A., Gerland, S., Haapala, J., Hudson, S. R., Johansson, A. M., King, J., Merkouriadi, I., Peterson, A. K., Provost, C., Randelhoff, A., Rinke, A., Rösel, A., Sennéchael, N., Walden, V. P., Duarte, P., Assmy, P., Steen, H., and Granskog, M. A.: Winter storms accelerate the demise of sea ice in the Atlantic sector of the Arctic Ocean, Scientific Reports, 9, 9222, https://doi.org/10.1038/s41598-019-45574-5, 2019.

Grieger, J., Leckebusch, G. C., Raible, C. C., Rudeva, I., and Simmonds, I.: Subantarctic cyclones identified by 14 tracking methods, and their role for moisture transports into the continent, Tellus A: Dyn. Meteorol. Oceanogr., 70, 1–18, https://doi.org/10.1080/16000870.2018.1454808, 2018.

Hepworth, E., Messori, G., and Vichi, M.: Association between extreme atmospheric anomalies over Antarctic sea ice, Southern Ocean polar cyclones and atmospheric rivers, Journal of Geophysical Research: Atmospheres, 127, e2021JD036 121, https://doi.org/10.1029/2021JD036121, 2022.

Hepworth, E., Messori, G., and Vichi, M.: Synoptic-scale extreme variability of winter Antarctic sea-ice concentration and its link to Southern Ocean extratropical cyclones, J. Geophys. Res. Oceans, 129, e2023JC019 825, https://doi.org/10.1029/2023JC019825, 2024.

Hibler III, W. D.: A dynamic thermodynamic sea ice model, J. Phys. Oceanogr., 9, 815–846, 1979.

Himmich, K., Vancoppenolle, M., Madec, G., Sallée, J.-B., Holland, P. R., and Lebrun, M.: Drivers of Antarctic sea ice advance, Nat. Commun., 14, 6219, https://doi.org/10.1038/s41467-023-41962-8, 2023.

Hobbs, W., Spence, P., Meyer, A., Schroeter, S., Fraser, A. D., Reid, P., Tian, T. R., Wang, Z., Liniger, G., Doddridge, E. W., and Boyd, P. W.: Observational evidence for a regime shift in summer Antarctic Sea Ice, J. Clim., 37, 2263–2275, https://doi.org/10.1175/JCLI-D-23-0479.1, 2024.

Holland, M. M., Bitz, C. M., Tremblay, L.-B., and Bailey, D. A.: The role of natural versus forced change in future rapid summer Arctic ice loss, in: Arctic Sea Ice Decline: Observations, Projections, Mechanisms, and Implications, edited by DeWeaver, E. T., Bitz, C. M., and Tremblay, L.-B., pp. 133–150, American Geophysical Union, Washington, D.C., ISBN 978-1-118-66647-0 978-0-87590-445-0, https://doi.org/10.1029/180GM10, 2008.

Horvat, C. and Tziperman, E.: A prognostic model of the sea-ice floe size and thickness distribution, The Cryosphere, 9, 2119–2134, https://doi.org/10.5194/tc-9-2119-2015, 2015.

Horvat, C., Tziperman, E., and Campin, J.-M.: Interaction of sea ice floe size, ocean eddies, and sea ice melting, Geophys. Res. Lett., 43, 8083–8090, https://doi.org/10.1002/2016GL069742, 2016.

Hunke, E., Allard, R., Bailey, D. A., Blain, P., Craig, A., Dupont, F., DuVivier, A., Grumbine, R., Hebert, D., Holland, M., Jeffery, N., Jean-Francois Lemieux, Osinski, R., Rasmussen, T., Ribergaard, M., Roberts, A., Roy, F., Turner, M., and Worthen, D.: CICE-Consortium/CICE: CICE version 6.3.0, Tech. rep., Los Alamos National Lab.(LANL), Los Alamos, NM (United States), https://doi.org/10.5281/ZENODO.5423913, 2021.

Hunke, E. C. and Dukowicz, J. K.: An elastic–viscous–plastic model for sea ice dynamics, J. Phys. Oceanogr., 27, 1849–1867, https://doi.org/10.1175/1520-0485(1997)027<1849:AEVPMF>2.0.CO;2, 1997.

Jena, B., Bajish, C. C., Turner, J., Ravichandran, M., Anilkumar, N., and Kshitija, S.: Record low sea ice extent in the Weddell Sea, Antarctica in April/May 2019 driven by intense and explosive polar cyclones, npj Climate and Atmospheric Science, 5, 19, https://doi.org/10.1038/s41612-022-00243-9, 2022.

https://doi.org/10.5194/egusphere-2025-5209
Preprint. Discussion started: 11 February 2026

Josey, S. A., Meijers, A. J. S., Blaker, A. T., Grist, J. P., Mecking, J., and Ayres, H. C.: Record-low Antarctic sea ice in 2023 increased ocean heat loss and storms, Nature, 636, 635–639, https://doi.org/10.1038/s41586-024-08368-y, 2024.

Keay, K., Galea, A., Messmer, M., Pepler, A., Rudeva, I., and Simmonds, I.: The University of Melbourne cyclone detection and tracking algorithm, University of Melbourne, 2020.

Kimura, N., Onomura, T., and Kikuchi, T.: Processes governing seasonal and interannual change of the Antarctic sea-ice area, J. Oceanogr., https://doi.org/10.1007/s10872-022-00669-y, 2022.

Kiss, A. E., Hogg, A. M., Hannah, N., Boeira Dias, F., Brassington, G. B., Chamberlain, M. A., Chapman, C., Dobrohotoff, P., Domingues, C. M., Duran, E. R., England, M. H., Fiedler, R., Griffies, S. M., Heerdegen, A., Heil, P., Holmes, R. M., Klocker, A., Marsland, S. J., Morrison, A. K., Munroe, J., Nikurashin, M., Oke, P. R., Pilo, G. S., Richet, O., Savita, A., Spence, P., Stewart, K. D., Ward, M. L., Wu, F., and Zhang, X.: ACCESS-OM2 v1.0: a global ocean–sea ice model at three resolutions, Geosci. Model Dev., 13, 401–442, https://doi.org/10.5194/gmd-13-401-2020, 2020.

Kohout, A. L., Williams, M. J., Dean, S. M., and Meylan, M. H.: Storm-induced sea-ice breakup and the implications for ice extent, Nature, 509, 604–607, https://doi.org/10.1038/nature13262, 2014.

Kohout, A. L., Williams, M. J., Toyota, T., Lieser, J., and Hutchings, J. K.: In situ observations of wave-induced sea ice breakup, Deep Sea Research Part II: Topical Studies in Oceanography, 131, 22–27, https://doi.org/10.1016/j.dsr2.2015.06.010, 2016.

Kriegsmann, A. and Brümmer, B.: Cyclone impact on sea ice in the Central Arctic Ocean: a statistical study, The Cryosphere, 8, 303–317, https://doi.org/10.5194/tc-8-303-2014, 2014.

Lim, E.-P. and Simmonds, I.: Southern Hemisphere winter extratropical cyclone characteristics and vertical organization observed with the ERA-40 data in 1979–2001, J. Clim., 20, 2675–2690, https://doi.org/10.1175/JCLI4135.1, 2007.

Lukovich, J. V., Stroeve, J. C., Crawford, A., Hamilton, L., Tsamados, M., Heorton, H., and Massonnet, F.: Summer extreme cyclone impacts on Arctic sea ice, J. Clim., 34, 4817–4834, https://doi.org/10.1175/JCLI-D-19-0925.1, 2021.

Massom, R., Reid, P., Warren, S., Light, B., Perovich, D., Bennetts, L., Uotila, P., O'Farrell, S., Meylan, M., Meiners, K., et al.: The influence of ocean waves on Antarctic sea-ice albedo and seasonal melting, and physical-biological feedbacks, EGUsphere, 2025, 1–44, 2025.

Matear, R. J., O'Kane, T. J., Risbey, J. S., and Chamberlain, M.: Sources of heterogeneous variability and trends in Antarctic sea-ice, Nat. Commun., 6, 8656, https://doi.org/10.1038/ncomms9656, 2015.

McGraw, M. C., Blanchard-Wrigglesworth, E., Clancy, R. P., and Bitz, C. M.: Understanding the forecast skill of rapid Arctic sea ice loss on subseasonal time scales, J. Clim., 35, 1179–1196, https://doi.org/10.1175/JCLI-D-21-0301.1, 2022.

Meucci, A., Young, I. R., Hemer, M., Kirezci, E., and Ranasinghe, R.: Projected 21st century changes in extreme wind-wave events, Science Advances, 6, eaaz7295, https://doi.org/10.1126/sciadv.aaz7295, 2020.

Meylan, M. H., Bennetts, L. G., and Kohout, A. L.: In situ measurements and analysis of ocean waves in the Antarctic marginal ice zone, Geophys. Res. Lett., 41, 5046–5051, https://doi.org/10.1002/2014GL060809, 2014.

Mundi, C. and L'Ecuyer, T.: Is the modern Arctic marginal ice zone more susceptible to summer cyclones?, J. Clim., https://doi.org/10.1175/JCLI-D-24-0026.1, 2024.

Phillips, T.: Cyclone tracks for the region south of 60S for 1979–2018 derived from 6-hourly ERA-Interim reanalysis mean sea level pressure (MSLP) fields, https://doi.org/10.5285/D3B5D87D-C882-4FED-9D47-14C73BE43BCA, 2020.

Renfrew, I. A., Barrell, C., Elvidge, A. D., Brooke, J. K., Duscha, C., King, J. C., Kristiansen, J., Cope, T. L., Moore, G. W. K., Pickart, R. S., Reuder, J., Sandu, I., Sergeev, D., Terpstra, A., Våge, K., and Weiss, A.: An evaluation of surface meteorology and fluxes over the Iceland

https://doi.org/10.5194/egusphere-2025-5209
Preprint. Discussion started: 11 February 2026

and Greenland Seas in ERA5 reanalysis: the impact of sea ice distribution, Quarterly Journal of the Royal Meteorological Society, 147, 691–712, https://doi.org/10.1002/qj.3941, 2021.

Roach, L. A., Horvat, C., Dean, S. M., and Bitz, C. M.: An emergent sea ice floe size distribution in a global coupled ocean-sea ice model, J. Geophys. Res. Oceans, 123, 4322–4337, https://doi.org/10.1029/2017JC013692, 2018a.

Roach, L. A., Smith, M. M., and Dean, S. M.: Quantifying growth of pancake sea ice floes using images from drifting buoys, J. Geophys. Res. Oceans, 123, 2851–2866, https://doi.org/10.1002/2017JC013693, 2018b.

Roach, L. A., Bitz, C. M., Horvat, C., and Dean, S. M.: Advances in modeling interactions between sea ice and ocean surface waves, Journal of Advances in Modeling Earth Systems, 11, 4167–4181, https://doi.org/10.1029/2019MS001836, 2019.

Roach, L. A., Eisenman, I., Wagner, T. J. W., and Donohoe, A.: Asymmetry in the seasonal cycle of zonal-mean surface air temperature, Geophys. Res. Lett., 50, e2023GL103 403, https://doi.org/10.1029/2023GL103403, 2023.

Saha, S., Moorthi, S., Wu, X., Wang, J., Nadiga, S., Tripp, P., Behringer, D., Hou, Y.-T., Chuang, H.-y., Iredell, M., et al.: The NCEP climate forecast system version 2, J. Clim., 27, 2185–2208, https://doi.org/10.1175/JCLI-D-12-00823.1, 2014.

Schroeter, S., Hobbs, W., and Bindoff, N. L.: Interactions between Antarctic sea ice and large-scale atmospheric modes in CMIP5 models, The Cryosphere, 11, 789–803, https://doi.org/10.5194/tc-11-789-2017, 2017.

Shen, H. H., Ackley, S. F., and Hopkins, M. A.: A conceptual model for pancake-ice formation in a wave field, Ann. Glaciol., 33, 361–367, https://doi.org/10.3189/172756401781818239, 2001.

Simmonds, I. and Keay, K.: Variability of Southern Hemisphere extratropical cyclone behavior, 1958–97, J. Clim., 13, 550–561, https://doi.org/10.1175/1520-0442(2000)013<0550:VOSHEC>2.0.CO;2, 2000a.

Simmonds, I. and Keay, K.: Mean Southern Hemisphere extratropical cyclone behavior in the 40-Year NCEP–NCAR reanalysis, J. Clim., 13, 873–885, https://doi.org/10.1175/1520-0442(2000)013<0873:MSHECB>2.0.CO;2, 2000b.

Smith, G. A., Hemer, M., Greenslade, D., Trenham, C., Zieger, S., and Durrant, T.: Global wave hindcast with Australian and Pacific Island focus: from past to present, Geoscience Data Journal, 8, 24–33, https://doi.org/10.1002/gdj3.104, 2021.

Smith, M., Stammerjohn, S., Persson, O., Rainville, L., Liu, G., Perrie, W., Robertson, R., Jackson, J., and Thomson, J.: Episodic reversal of autumn ice advance caused by release of ocean heat in the Beaufort Sea, J. Geophys. Res. Oceans, 123, 3164–3185, https://doi.org/10.1002/2018JC013764, 2018.

Sprenger, M., Fragkoulidis, G., Binder, H., Croci-Maspoli, M., Graf, P., Grams, C. M., Knippertz, P., Madonna, E., Schemm, S., Škerlak, B., and Wernli, H.: Global climatologies of Eulerian and Lagrangian flow features based on ERA-Interim, Bulletin of the American Meteorological Society, 98, 1739–1748, https://doi.org/10.1175/BAMS-D-15-00299.1, 2017.

Tersigni, I., Alberello, A., Messori, G., Vichi, M., Onorato, M., and Toffoli, A.: High-resolution thermal imaging in the Antarctic marginal ice zone: skin temperature heterogeneity and effects on heat fluxes, Earth and Space Science, 10, e2023EA003 078, https://doi.org/10.1029/2023EA003078, 2023.

Thomas, S., Babanin, A. V., Walsh, K. J. E., Stoney, L., and Heil, P.: Effect of wave-induced mixing on Antarctic sea ice in a high-resolution ocean model, Ocean Dynamics, 69, 737–746, https://doi.org/10.1007/s10236-019-01268-0, 2019.

Tsujino, H., Urakawa, S., Nakano, H., Small, R. J., Kim, W. M., Yeager, S. G., Danabasoglu, G., Suzuki, T., Bamber, J. L., Bentsen, M., Böning, C. W., Bozec, A., Chassignet, E. P., Curchitser, E., Boeira Dias, F., Durack, P. J., Griffies, S. M., Haranda, Y., Ilicak, M., Josey, S. A., Kobayashi, C., Kobayashi, S., Komuo, Y., Large, W. G., Le Sommer, J., Marsland, S. J., Masina, S., Scheinert, M., Tomita, H., Valdivieso, M., and Yamazaki, D.: JRA-55 based surface dataset for driving ocean–sea-ice models (JRA55-do), Ocean Modelling, 130, 79–139, https://doi.org/10.1016/j.ocemod.2018.07.002, 2018.

https://doi.org/10.5194/egusphere-2025-5209
Preprint. Discussion started: 11 February 2026

Uotila, P., Vihma, T., Pezza, A. B., Simmonds, I., Keay, K., and Lynch, A. H.: Relationships between Antarctic cyclones and surface conditions as derived from high-resolution numerical weather prediction data, Journal of Geophysical Research, 116, D07 109, https://doi.org/10.1029/2010JD015358, 2011.

Vichi, M., Eayrs, C., Alberello, A., Bekker, A., Bennetts, L. G., Holland, D. M., de Jong, E., Joubert, W., MacHutchon, K., Messori, G., Mojica, J. F., Onorato, M., Saunders, C., Skatulla, S., and Toffoli, A.: Effects of an explosive polar cyclone crossing the Antarctic marginal ice zone, Geophys. Res. Lett., 46, 5948–5958, https://doi.org/10.1029/2019GL082457, 2019.

Vihma, T., Pirazzini, R., Fer, I., Renfrew, I. A., Sedlar, J., Tjernström, M., Lüpkes, C., Nygård, T., Notz, D., Weiss, J., Marsan, D., Cheng, B., Birnbaum, G., Gerland, S., Chechin, D., and Gascard, J. C.: Advances in understanding and parameterization of small-scale physical processes in the marine Arctic climate system: a review, Atmospheric Chemistry and Physics, 14, 9403–9450, https://doi.org/10.5194/acp-14-9403-2014, 2014.

Wang, Z., Walsh, J., Szymborski, S., and Peng, M.: Rapid Arctic sea ice loss on the synoptic time scale and related atmospheric circulation anomalies, J. Clim., 33, 1597–1617, https://doi.org/10.1175/JCLI-D-19-0528.1, 2020.

Womack, A., Vichi, M., Alberello, A., and Toffoli, A.: Atmospheric drivers of a winter-to-spring Lagrangian sea-ice drift in the Eastern Antarctic marginal ice zone, Journal of Glaciology, 68, 999–1013, https://doi.org/10.1017/jog.2022.14, 2022.

Womack, A., Alberello, A., de Vos, M., Toffoli, A., Verrinder, R., and Vichi, M.: A contrast in sea ice drift and deformation between winter and spring of 2019 in the Antarctic marginal ice zone, The Cryosphere, 18, 205–229, https://doi.org/10.5194/tc-18-205-2024, 2024.

Young, I. R., Fontaine, E., Liu, Q., and Babanin, A. V.: The wave climate of the Southern Ocean, J. Phys. Oceanogr., 50, 1417–1433, https://doi.org/10.1175/JPO-D-20-0031.1, 2020.

Zhang, J., Lindsay, R., Schweiger, A., and Steele, M.: The impact of an intense summer cyclone on 2012 Arctic sea ice retreat, Geophys. Res. Lett., 40, 720–726, https://doi.org/10.1002/grl.50190, 2013.

Zhang, L., Ren, X., Wang, C.-Y., Gan, B., Wu, L., and Cai, W.: An observational study on the interactions between storm tracks and sea ice in the Southern Hemisphere, Climate Dynamics, 62, 17–36, https://doi.org/10.1007/s00382-023-06894-5, 2024.